A new global dataset of mountain glacier centerline and length

Dahong Zhang [1,2], Gang Zhou [1,2], Wen Li [1,2], Shiqiang Zhang [1,2], Xiaojun Yao [3], Shimei Wei [3]

[1] College of Urban and Environmental Science, Northwest University, Xi'an 710127, PR China

[2] Shaanxi Key Laboratory of Earth Surface System and Environmental Carrying Capacity, Northwest University, Xi'an 710127, PR China

[3] College of Geography and Environment Sciences, Northwest Normal University, Lanzhou 730070, PR China

Correspondence: Shiqiang Zhang (zhangsq@lzb.ac.cn)

Abstract. Length is one of the key determinants of glacier geometry and is an important parameter of glacier inventory and modeling; glacier centerlines are crucial inputs for many glaciological applications. In this study, the centerlines and maximum lengths of global glaciers were extracted using an automatic extraction algorithm based on the latest global glacier inventory data, digital elevation data (DEM), and European allocation theory. The glacier polygons were reconstructed according to the geometric principle and an automatic checking algorithm for the global glacier outlines was designed to filter erroneous or unsupported glacier outlines. The DEMs of global glacier-covered regions were compiled using available DEMs. An updated automatic extraction tool was designed independently, and a parameterization scheme with empirical thresholds was applied for data production. The accuracy of the dataset was evaluated using random assessment with visible interpretation and comparative analysis with another dataset. The 10,764 erroneous glacier polygons, 7,174 ice caps, and 419 nominal glaciers from the Randolph Glacier Inventory (RGI) version 6.0 were identified and excluded, accounting for 8.25% of the total. In total, 198,137 glacier centerlines were generated, accounting for 99.74% of the total input glaciers and 91.52% of the RGI v6.0. The accuracy of glacier centerlines was 89.68%. The comparison between the dataset and previous datasets suggested that the majority of glacier centerlines were slightly longer than those in RGI v6.0. The extraction method of this study has a strong ability to obtain the maximum length of glaciers, meaning that the maximum lengths of some glaciers were likely underestimated in the past. The dataset constructed includes ~~14~~ 17 sub-datasets, such as the global glacier centerline dataset, global glacier maximum length dataset, and global glacier DEM dataset, all of which can be found at link: https://doi.org/10.11922/sciencedb.01643 (Zhang and Zhang, 2022).

1 Introduction

Mountain glaciers which are distinct from the Greenland and Antarctic ice sheets, are also shrinking rapidly (Hugonnet et al., 2021). They are altering regional hydrology (Pritchard, 2019), raising global sea levels (Cazenave, 2018), and elevating natural hazards (Shukla and Sen, 2021; Zheng et al., 2021). These glaciers are among the most climate-sensitive constituents of the world's natural water towers (Immerzeel et al., 2019). Under the influence of global climate change, studies on glacier area changes (Sommer et al., 2020; Li et al., 2021), ice thickness (Farinotti et al., 2019), mass balance (Zemp et al., 2019; Vargo et al., 2020; Wu et al., 2021), ice velocity field (Thogersen et al., 2019), the impact of debris-cover (Scherler et al., 2018; Shukla et al., 2020; Herreid and Pellicciotti, 2020), glacier meltwater (Noel et al., 2020), sediment release (Aciego et al., 2015; Li et al., 2019), and related hazards (Zhou et al., 2021b; Stuart-Smith et al., 2021; Kääb et al., 2021) in glacier-covered regions are essential for global water resources supply and disaster prevention and reduction.

The most obvious distinction between glaciers and other natural ice bodies is their property to move towards lower altitudes under the influence of gravity. Glacier flow lines are the motion trajectories of a glacier and the main flow line is the key trajectory. The main flow line cannot be obtained on a large scale owing to the lack of glacier velocity field data. The glacier centerline, generated via the axis line method (Le Bris and Paul, 2013; Machguth and Huss, 2014; Kienholz et al., 2014; Zhang et al., 2021), is typically used to represent the main flow line. The glacier centerline is a critical parameter for analyzing the ice velocity field (Heid and Kääb, 2012; Melkonian et al., 2017), estimating the glacier volume (Li et al., 2012; Gao et al., 2018), and developing glacier models (Oerlemans, 1997; Sugiyama et al., 2007; Maussion et al., 2019).

Glacier length, usually referring to the maximum length of a glacier centerline (main flow line), represents the longest motion trajectory of a glacier, which is one of the key determinants of glacier geometry and a basic parameter of glacier inventories (RGI Consortium, 2017) and modeling (Maussion et al., 2019). Glacier length fluctuations can be used to quantify glacier changes (Zhou et al., 2021a), such as by identifying glacier advancement, surge, or retreat. Glacier length fluctuations (e.g., Leclercq et al., 2014) have also been used to study the relationships with changes in glacier area (Winsvold et al., 2014) and the geometric structure of a glacier (Herla et al., 2017), estimate glacier volume in combination with the glacier area (Lüthi et al., 2010), and reconstruct annual averaged surface temperatures over the past 400 years on hemispherical and global scales (Leclercq and Oerlemans, 2011).

The global complete inventory (RGI Consortium, 2017) of glacier outlines was created following the Fifth Assessment Report of the Intergovernmental Panel on Climate Change (IPCC AR5). To meet the demand for large-scale acquisition of glacier length, automatic and semi-automatic methods have been proposed. There are three types of methods: first, the typical hydrological analysis method (Schiefer et al., 2008), but the lengths are longer than equivalent maximum distances taken along typical longitudinal centerline profiles; second, a simplified algorithm based on skeleton theory (Le Moine and Gsell, 2015), but this method has not been widely used; third, centerline method based on the axis concept, proposed by Le Bris and Paul (2013), and applied to the calculation of global glacier length for the first time by Machguth and Huss (2014). However, it is difficult to extract complex glaciers using the method ~~of~~ (Le Bris and Paul, 2013). The cost grid-least-cost route approach of Kienholz et al. (2014) based on the axis concept has higher accuracy, but it requires more labor and time, which limits its application to global glaciers. The trade-off function approach of Machguth and Huss (2014) was based on the axis concept~~;~~, ~~the~~ their results cover almost all mountain glaciers in the world but exclude the centerlines of branches of glaciers. Therefore, researchers have been trying to overcome these difficulties in recent years (Yao et al., 2015; Yang et al., 2016; Ji et al., 2017; Hansen et al., 2020; Xia, 2020; Zhang et al., 2021). To date, global datasets of the centerline and length of mountain glaciers are rare, including that of glacier branches. Based on our recent study (Zhang et al., 2021) on successfully extracting the glacier centerline using the Euclidean allocation, in this study, we aim to combine free, available digital elevation data into one global digital elevation model (DEM) with 30 m resolution from 90°N to 90°S, check and correct the global glacier outlines, and obtain a new graphic dataset of the centerline and length for global mountain glaciers based on the updated DEM and outlines.

2 Study region and data

The glacier dataset used in this study was the RGI version 6.0 (http://www.glims.org/RGI/randolph.html, last accessed: 15 November 2021) released via the Global Land Ice Measurements from Space initiative (GLIMS), which is a globally complete collection of digital outlines of glaciers, excluding ice sheets (Pfeffer et al., 2014). RGI v6.0 includes 216,502 glaciers (215,547 glaciers described in the product handbook) worldwide, with a total area of 705,738.793 km^2 (RGI Consortium, 2017). All glaciers can be divided into 19 first-order glacier regions (Radić and Hock, 2010), and these regions were used in our study (Fig. 1).

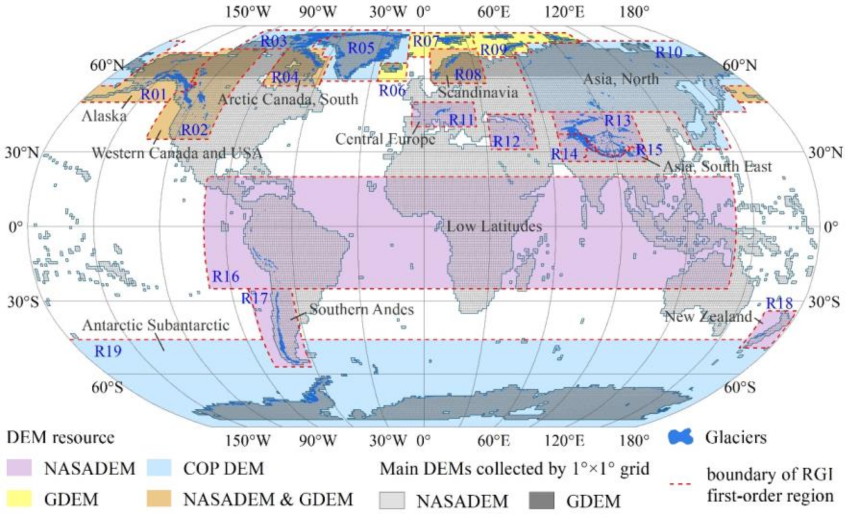

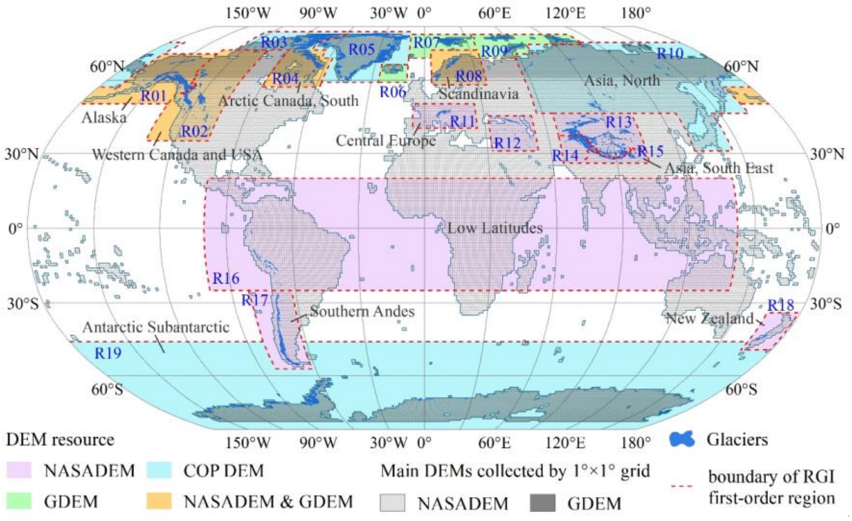

Figure 1. Distribution of global glaciers, first-order glacier regions, and DEMs. The background is

the global DEM grid (1°×1°) covered by NASADEM and GDEM. GDEM and COP DEM represent the ASTER GDEM v3 and the Copernicus DEM, respectively. **Notes:** R03: Arctic Canada, North; R05: Greenland Periphery; R06: Iceland; R07: Svalbard and Jan Mayen; R09: Russian Arctic; R12: Caucasus and Middle East; R13: Asia, Central; R14: Asia, South West.

设置了格式：字体：加粗

Five DEM products (Table 1) were collected in preliminary studies. The National Aeronautics and Space Administration (NASA) DEM (NASADEM) (https://lpdaac.usgs.gov/news/release-nasadem-data-products/, last accessed: November 17, 2021) was released by the Land Processes Distributed Active Archive Center (LP DAAC) in January 2020. As a modernization of the DEM and associated products generated from the Shuttle Radar Topography Mission (SRTM) data (Farr et al., 2007), the NASADEM, with a low mean absolute error (MAE) (Carrera-Hernández, 2021), is the successor of the NASA SRTM V3. The root mean square error (RMSE) of NASADEM is ~~better~~smaller than that of SRTM (Uuemaa et al., 2020). Serving the zonal extent of (56°S, 61°N), NASADEM was used as the preferred DEM in this study because of its superior performance. The Advanced Spaceborne Thermal Emission and Reflection Radiometer (ASTER) is a 14-channel imaging instrument operating on the Terra satellite of NASA since 1999. ASTER Global Digital Elevation Model (GDEM) version 3 (https://lpdaac.usgs.gov/news/nasa-and-meti-release-aster-global-dem-version-3/, last accessed: November 17, 2021) (Abrams et al., 2020) was released by Japan's Ministry of Economy, Trade, and Industry (METI) and NASA in July 2019. Using ICESat data, Carabajal and Boy (2016) found that ASTER GDEM v3 displayed smaller means, similar medians, and less scatter than ASTER GDEM v2 in Greenland and Antarctica. To determine the zonal extent of (56°S, 83°S) and (61°N, 83°N), ASTER GDEM v3 was used as the second priority DEM in this study.

NASADEM and ASTER GDEM v3 do not cover all glacierized regions, missing parts of the polar region and the Kamchatka Peninsula. Because of their high temporal and spatial resolution at high latitudes, the reference elevation model of Antarctica (REMA) (Howat et al., 2019) and ArcticDEM (https://www.pgc.umn.edu/data/arcticdem/, last accessed: November 17, 2021) were preferred as the supplementary data of our preliminary studies in these glacier regions. ~~However~~Nevertheless, ArcticDEM and REMA are not suitable because of insufficient coverage and sporadic data. Therefore, Copernicus DEM (https://spacedata.copernicus.eu/web/cscda/cop-dem-faq, last accessed: November 17, 2021) with a wide coverage was finally determined as the supplementary data for glacier regions not covered via the NASADEM and ASTER GDEM v3 completely. The Copernicus DEM was recently released (November 2020) and the accuracy assessment undertaken by its development team (the product handbook) using TanDEM-X DEM/World DEM ICESat GLAS reference points found an absolute vertical accuracy of approximately 10 m at the periphery of Antarctica and Greenland. Finally, NASADEM, ASTER GDEM v3, and Copernicus DEM were compiled to create a 30 m DEM of the completely covered study area.

Table 1. All DEMs collected in this study

DEM	Extent	Resolution	Access
NASADEM	[56°S, 61°N]	30 m	https://search.earthdata.nasa.gov/search
ASTER GDEM v3	[83°S, 83°N]	30 m	https://gdemdl.aster.jspacesystems.or.jp/
ArcticDEM	[55°N, 90°N]	2 m	https://earthengine.google.com/
REMA	[60°S, 88°S]	2m / 8m	https://earthengine.google.com/
Copernicus DEM	Global	30 m	https://panda.copernicus.eu/web/cds-catalogue/panda

Note: The interval in the 'Extent' column represents all landmasses within a zonal range, but coverage may not exist for all areas.

In addition, graphical data (Machguth and Huss, 2014) of glacier length in *. xy format with an unknown projection coordinate system in High Asia were collected, which correspond to the attribute of the glacier maximum length (L_{max}) in RGI v6.0. Because the data was obtained from an unofficial source, we could not access the data description documents and only recovered the coordinate matching between these points and some glaciers in RGI v6.0. Registration of the *. xy file depends on the match between its filename and the feature identity document (FID) of the glacier polygon of RGI v6.0 in the same glacier area. The glacier lengths (*MHMLDS*) of successful registration were used as graphical validation data for this study.

3 Methods

3.1 Outline of workflow

This study relied on two key input datasets: global glacier inventory and compiled global glacier elevation. The goal of this study was to establish a new dataset of global graphic glacier centerlines and lengths. An outline of the workflow is shown in Figure 2. The process was divided into six parts: (1) design an algorithm to check all glacier outlines, marks, and exclude defective glacier polygons; (2) buffer glaciers to produce a mask containing global glaciers and their buffers; (3) mosaic compiled global DEMs according to the masks in step 2 of different glacier regions to prepare the global glacier elevation data; (4) determine the automatic extraction parameters of glacier centerlines around the world by repeated testing in each region; (5) input the global DEM and glacier outline dataset and all parameters into the designed automatic extraction software (Zhang et al., 2021) to generate the centerlines and length in the global glacier; and (6) verify and compare with other centerline results obtained via different methods to evaluate the accuracy of the new datasets.

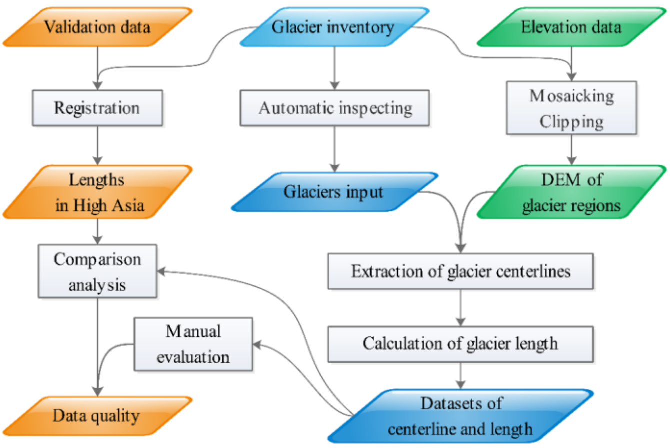

Figure 2. Workflow of the centerline and length dataset production.

3.2 Illustration of key methods

3.2.1 Pre-process of glacier outlines

This study had strict requirements for glacier outlines, and all glacier complexes should be divided into individual glaciers before centerline extraction. However, because of the limited semi-automatic glacier segmentation approach (Kienholz et al., 2013) and the high-priority strategy of completeness of coverage adopted by RGI v6.0 (RGI Consortium, 2017), some glaciers were not supported by our algorithm. These glaciers included three categories: glacier complexes with/without inaccurate segmentation (Fig. 3a-b), incorrect glacier outlines (Fig. 3c), and flawed glaciers (Fig. 3d-f) generated by the automatic extraction algorithm. For the third category, we designed an identification algorithm (see paragraph 3) to mark and screen them. The flaws in these glacier outlines were mainly caused by topology errors of polylines/polygons, such as unclosed, sawtooth, and overlap. The first two categories do not affect the program's normal operation; however, the accuracy of the extraction results is difficult to guarantee. We cannot identify them at present and a solution is needed to improve the quality of the global glacier inventory.

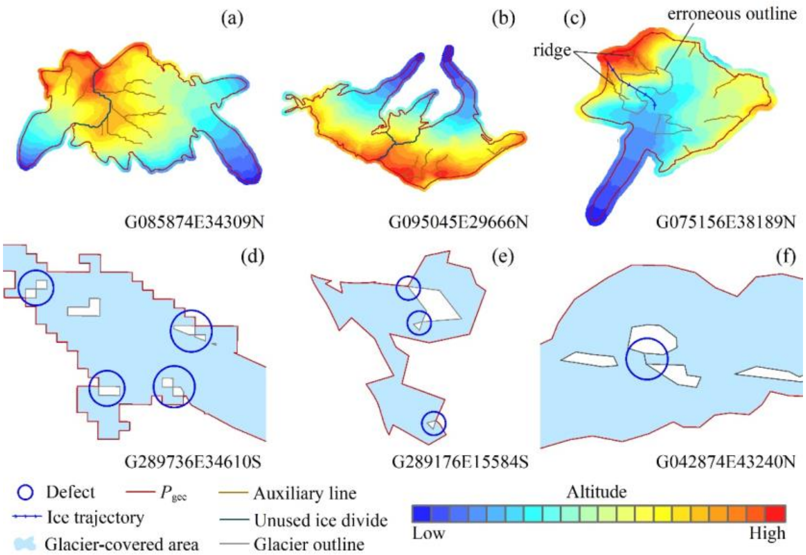

Figure 3. Schematic of three types of flawed glacier outlines. **(a-b)** Glacier complexes with/without inaccurate segmentation. **(c)** Incorrect glacier outline. **(d-f)** Panels represent three common problems in flawed glaciers: defects in automatic algorithm, defects in post-processing, and artificial errors. Auxiliary line represents lower-grade ice divide in the individual glacier, which is part of the ridge lines.

In this study, we defined the external contour of a glacier (P_{gec}), namely, the polygon corresponding to the longest closed polyline of the glacier, to reduce the storage of DEMs and improve the efficiency of batch processing. The buffer masks of all glaciers (buffer distance: approximately 100 m) were generated by their P_{gec} to meet the requirement for the extent of input DEMs to be slightly larger than the P_{gec}. The buffer masks generated initially were relatively broken because there are overlaps or gaps between the adjacent polygons of the buffer zone. We merged small spots to remove polygons with a perimeter less than 12 times the buffer distance on the glacier buffer masks of each region.

The third category of glaciers (Fig. 3d-f) with flaws was identified by obtaining P_{gec}. In the third category, the most common type is two or more closed polylines with the same endpoint in a glacier. There were also a few glacier polygons with false closed polylines, which are the head and tail endpoints of the polylines that do not coincide, but the distance is less than the tolerance. The solution ~~was~~ are as follows: flawed glacier outlines were identified by judging whether there were multiple polylines sharing endpoints after converting the glacier from a polygon to polylines, but these outlines do not include the false closed type.

3.2.2 Preparation of input datasets

All data were processed in units of first-order glacier regions. The input glacier outlines excluded all the defective glacier outlines. Similarly, the nominal glaciers (represented by an ellipse) and ice caps remarked in RGI v6.0 were also treated, which were distinguished by two attributes: status (nominal glacier) and form (ice cap). The inspection results (Table 2) of glacier outlines show that there are 10,764 defective glacier outlines (*FGODS*) in RGI v6.0, accounting for approximately 4.97% of the total (216,502). After excluding nominal glaciers (461) and ice caps (7,174), 198,646 glaciers remained as input glacier outlines (*IGODS*), accounting for 91.75% of the ~~total~~ global mountain glaciers.

Table 2. Preprocessing results of different glacier regions and information of input datasets.

Region	Region Name	Total	Ice Cap	Nominal glacier	Flawed glacier	Glacier input	DEM input
R01	Alaska	27108	0	0	704	26404	NASADEM, GDEM
R02	Western Canada and USA	18855	0	0	1564	17291	NASADEM, GDEM
R03	Arctic Canada, North	4556	650	0	47	3869	COP DEM
R04	Arctic Canada, South	7415	953	0	63	6409	NASADEM, GDEM
R05	Greenland Periphery	20261	1658	0	1547	17247	COP DEM
R06	Iceland	568	133	0	1	435	GDEM
R07	Svalbard	1615	144	0	12	1460	GDEM
R08	Scandinavia	3417	0	4	75	3338	NASADEM, GDEM
R09	Russian Arctic	1069	460	0	0	609	GDEM
R10	North Asia	5151	5	116	136	4899	COP DEM
R11	Central Europe	3927	0	2	76	3849	NASADEM
R12	Caucasus Middle East	1888	0	339	2	1547	NASADEM
R13	Central Asia	54429	1545	0	28	52858	NASADEM
R14	South Asia West	27988	295	0	1946	25792	NASADEM
R15	South Asia East	13119	289	0	4	12826	NASADEM
R16	Low Latitudes	2939	0	0	724	2215	NASADEM
R17	Southern Andes	15908	623	0	3828	11734	NASADEM
R18	New Zealand	3537	0	0	0	3537	NASADEM
R19	Antarctic Subantarctic	2752	419	0	7	2327	COP DEM
--	--	216502	7174	461	10764	198646	--

Note: GDEM and COP DEM represent ASTER GDEM v3 and Copernicus DEM, respectively.

P_{gec} of all glaciers in RGI v6.0 constitute the global glacier external contour dataset (*GGECDS*), which generated the buffer mask dataset (*GGBMDS*) of global mountain glaciers. The collected DEMs were extracted using *GGBMDS* and 43,035 DEM tiles were generated. They were then mosaicked according to different first-order glacier regions to generate a global glacier elevation dataset (*GGEDS*). The details of the two input datasets are presented in Table 2.

3.2.3 Generation of centerline and glacier length

The automatic extraction tool of 'GlacierCenterlines_Py27' (Update to version 5.2.1) was used, which is based on the axis concept and Euclidean allocation (Zhang et al., 2021). The principle is briefly explained as follows: the highest and lowest points of the external outline of a glacier as two endpoints were extracted, cells with the equal shortest distances from the cell to both sides were identified in a glacier polygon, and the line formed by these cells was regarded as the glacier centerline. The maximum length of ~~a~~ glaciers was calculated using an algorithm similar to the critical path. The updated contents focused on formulating the parameterization scheme (Appendix A: Table A1) for extracting global glacier centerlines, as well as repairing some newly discovered bugs, such as a dead cycle in the process of auxiliary line extraction. All glacier outlines included in the *IGODS* were divided into ten levels (Table 3) using the proportion of cumulative area after ranking the area of all input glacier polygons from small to large. User-defined Albers with WGS1984 as the reference ellipsoid were used as a unified projection coordinate system. The central meridian, standard parallel 1, standard parallel 2, and origin latitude of the different glacier regions were determined by their spatial extent. The empirical values of the other parameters were determined in repeated attempts and their values had a significant correlation with glacier scale. The glacier centerlines generated were merged according to the glacier regions and the graphics and attribute information of glacier length were exported as corresponding independent ESRI shapefiles. In addition, some key associated data were exported, such as the segmentation results of glacier outlines, the lengths in the accumulation and ablation region of each glacier, the lowest points, the local highest points (P_{max}), the failed glacier outlines dealt, and logs.

Table 3. Statistics of global glaciers by different levels.

Level	Count	Area/km^2	Acc. area/km^2	Percent	Interval/km^2
L1	165593	1.00	41313.79	10%	[0.01, 1.00]
L2	22833	3.57	82629.47	20%	(1.00, 3.57]
L3	6906	11.39	123947.69	30%	(3.57, 11.39]
L4	2149	35.51	165282.14	40%	(11.39, 35.51]
L5	698	103.10	206631.32	50%	(35.51, 103.10]
L6	262	248.26	247917.55	60%	(103.10, 248.26]
L7	113	521.40	289227.71	70%	(248.26, 521.40]
L8	55	1087.47	330595.34	80%	(521.40, 1087.47]
L9	27	2657.74	374312.14	90%	(1087.47, 2657.74]
L10	10	6004.85	413136.71	100%	(2657.74, 6004.85]
Total	198646	--	--	--	--

3.2.4 Accuracy assessment

A random assessment was prioritized in this study. We randomly selected 100 glaciers in each glacier region and obtained 19 samples with a total of 1,900 glacier centerlines. These glacier centerlines were divided by artificial inspection into three first-level categories (Zhang et al., 2021): correct (I), inaccurate (II), and incorrect (III). Type II mostly contains glaciers with accurate glacier maximum lengths but missing, redundant, or unreasonable branches of glacier centerlines. When calculating verification accuracy, Types I and II were regarded as correct, and only Type III was considered incorrect. Finally, the glacier proportion of Type III in the sample was counted and the valuation result (R) was calculated using Eq. (1).

$$R = \sum_{i=1}^{19} \frac{S_i \times N_{T_i}}{N_G} \quad , (1)$$

where N_G is the total quantity of glaciers and N_{Ti} and S_i are the verification accuracy and number of glaciers in the corresponding glacier region of the *i* th sample (i = 1, 2, 3, ..., 18,19), respectively. All glacier maximum lengths (G_{Lmax}) in this study were compared with the $L_{\max}$ (Machguth and Huss, 2014) in RGI v6.0 using linear correlation and ratio analysis. Here, we took L_4 - L_{10} at the glacier level as the same grade for statistics. The correlations between G_{Lmax} and $L_{\max}$ were established according to different glacier regions and glacier levels and the length ratio, R_r (Eq. 2), was calculated. In addition, considering the differences between the graphics, we also collected graph data of glacier length extracted by Machguth and Huss (2014). Considering the limited availability of data (obtained: R13–R15), we only compared two glacier-covered regions in the Himalayas: Mount Qomolangma and Kangchenjunga (the world's third-highest mountain) and their surrounding areas.

$$\mathrm{R}_r = \frac{G_{L\max}}{L_{\max}} \qquad (2)$$

4 Results

4.1 Centerline and length of glaciers

Taking the *IGODS*, *GGEDS*, and other model parameters as input data, 198,137 glacier centerlines were automatically generated using the centerline extraction tool of 'GlacierCenterlines_Py27 v5.2.1', with an overall success rate of 99.74%. The number and proportion of flawed glacier outlines, nominal glaciers, ice caps, input glacier outlines, and extraction results for distinct glacier regions are shown in Fig. 4.

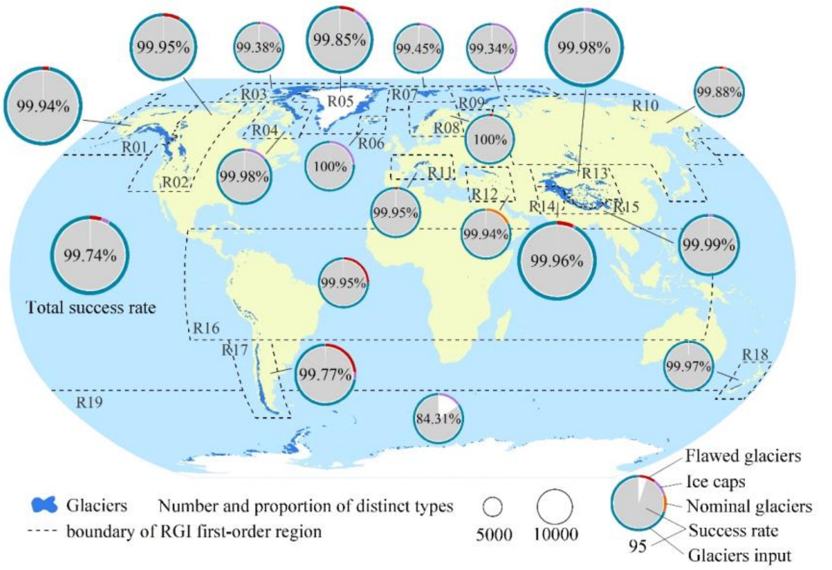

Figure 4. Extraction results of glacier centerlines in different glacier regions. The ring in the pie chart represents the proportion of input glacier number and the number of excluded three glacier types with total number of glaciers in the region. Pie chart represents the correct rate, which is the proportion of the extraction result number with input glacier quantity. The size of the pie/ring represents the grade of the glacier number in the region.

Except for Antarctica and Subantarctica (R19), the success rates of extracting glacier centerlines in other glacier regions were greater than 99%, which indicates that the automatic extraction algorithm for glacier centerlines is robust. A small number of glacier outlines with false closed problems and unidentified ice caps were the main reasons for the failure of automatic extraction of glacier centerlines; however, it is difficult to establish rules for accurately identifying these glacier polygons. In total, 510 unsuccessful glacier outlines were identified, of which Antarctic-Subantarctic (R19) accounted for 71.57%; Southern Andes (R17) and Greenland Periphery (R05) for 5.29% and 5.1%, respectively; Arctic Canada North (R03) and Alaska (R01) for 4.71% and 2.94%, respectively; and other glacier regions for less than 2%.

Overall, the global glacier centerline dataset (*GGCLDS*) constructed in this study contained 91.52% of the total glaciers in RGI v6.0. The lengths of each branch of the glacier centerline were derived and the longest branch lengths of the glacier centerline were defined as the glacier maximum length (G_{Lmax}), which were used to form the global glacier maximum length dataset (*GGMLDS*). The average centerline length of all branches of a glacier is called the glacier mean length (G_{Lmean}). In addition, the median glacier altitude was regarded as the equilibrium line altitude (ELA) (Machguth and Huss, 2014), the part with G_{Lmax} higher than ELA was regarded as the length of the glacier accumulation zone (G_{Lacc}), and the part lower than ELA was regarded as the length of the glacier ablation zone (G_{Labl}), which formed the glacier accumulation zonal length dataset (*GACLDS*) and glacier ablation zone length dataset (*GABLDS*). The key process data corresponding to *GGCLDS* were also output, to form the glacier outline segmentation results (*GOSRDS*), lowest points (*GGLPDS*), local highest points (*GLHPDS*), and unsuccessful glacier outlines (*GUGODS*). The fields involved in all datasets are explained in Table 4.

Table 4. Description of the attributes contained in all datasets.

Name	Data type	Char. length	Description
GLIMS_ID	Char.	14	Unique code of a glacier
Type	Long int.	4	Glacier grade in this study
MaxL	Float	8	Glacier maximum length (Unit: m)
MeanL	Float	8	Glacier average length (Unit: m)
ELA	Long int.	4	Equilibrium line altitude (Unit: m)
AccL	Float	8	Length in the accumulation region (Unit: m)
AblationL	Float	8	Length in the ablation region (Unit: m)
Id	Long int.	8	Data code of the same glacier
BS	Long int.	8	Tag of the same segment in a glacier
RASTERVALU	Long int.	4	Altitude of a $P_{\max}$ (Unit: m)

Note: Char. and int. represent Character and integer, respectively.

The glacier outlines of RGI v6.0 without centerline results in this study were limited by the quality of the glacier polygons, which mainly correspond to the flawed glacier outlines *(FGODS*), and the identified ice caps in RGI v6.0 (Table 2). Among the *FGODS* (10,764), Southern Andes (R17) had the most, followed by Southwest Asia (R14); Western Canada and USA (R02) and Greenland Periphery (R05), with slightly more than 1,500; and Low Latitudes (R16) and Alaska (R01), with slightly more than 700. There were 451 in other glacier regions, including two regions with 0 defective glacier outline, the Russian Arctic (R09) and New Zealand (R18). Among the ice caps (7174) identified by RGI v6.0, slightly more than 1,500 were in R05 and Central Asia (R13), between 500 and 1,000 in the Arctic Canada South (R04), Arctic Canada North (R03), and R17, and less than 500 in other glacier regions. Nominal glaciers (461) existed in three glacial regions: Caucasus Middle East (R12), North Asia (R10), and Scandinavia (R08).

4.2 Data validation

4.2.1 Random self-assessment results

The evaluation results using random samples from the glacier centerline dataset suggested that the average verification accuracy of the glacier centerline dataset was 89.68%. There were significant differences in the accuracy of the 19 glacier regions around the world (Fig. 5). Among them, R11, R15 and R10, R09, and R19 were the highest (98%), second highest (95%), slowest lower (78%), and lowest (50%), respectively. In terms of types, the average proportions of Types I and II were 83.53% and 6.16%, respectively. The proportion of Type I in R07 and R09 was relatively low, at 79% and 73%, respectively, and the lowest in R19 was only 50%. Type II had the highest proportion in R19 at 16%, followed by R07 (10%). Moreover, Type II accounted for more than 5% in seven regions: R11, R13, R17, R18, R16, R01, and R06.

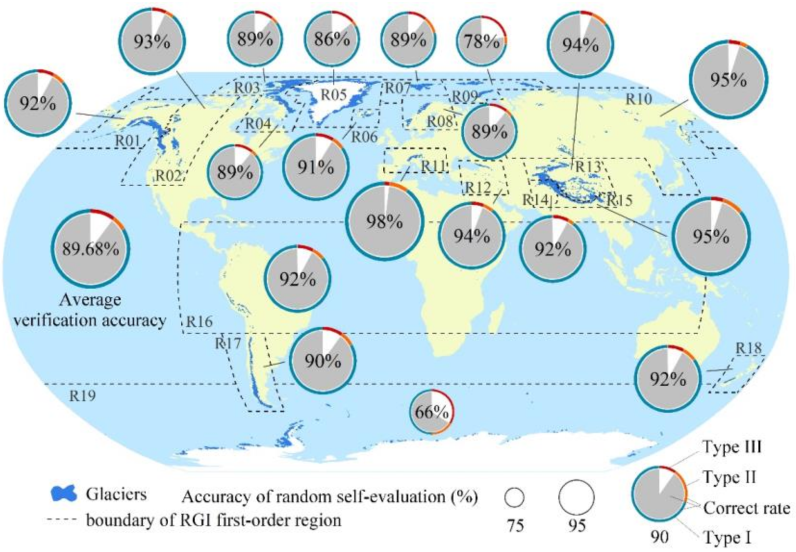

Figure 5. Statistical chart of random evaluation results. The ring in the pie chart represents the proportion of each type with total number of samples in the region. Pie chart represents the correct rate, which is the proportion of the number of Types I and II with region sample quantity. The size of the pie/ring represents the grade of the correct rate in the region. Types I, II, and III (See Section 3.2.4) represent the centerline of correct, inaccurate, and incorrect, respectively.

The above results indicate that, in addition to the three glacier regions of R07, R09, and R19, the random samples of the glacier centerline dataset have excellent performance in terms of accuracy, particularly in R02, R12, and R14. The unmarked ice cap and local low-quality DEM were the main reasons for the poor quality of the glacier centerline in R07 and R09, respectively. Owing to glacier complexes and low altitude differences in low-quality DEMs at the glacier tongue, the quality of the glacier centerline obtained in R19 was poor. However, from the viewpoint of dataset coverage, we provided the extraction results of the glacier centerline in R19.

4.2.2 Compare with previous results

After applying this algorithm to the global glacier inventory RGI v6.0, we compared the glacier lengths (G_{Lmax}) automatically obtained in this study with those (L_{max}) obtained by Machguth and Huss (2014) (Fig. 6). After eliminating 5408 glaciers with L_{max} value of -9 (no results), the length values of the other 192728 glaciers in the global glacier length dataset were directly compared. The G_{Lmax} and L_{max} were generally comparable (Fig. 6a). The glaciers in grades L_4–L_{10} showed excellent fitting degrees, while those of L_1–L_3 determined the linear correlation coefficient owing to their large number. The number of glaciers with a length ratio (R_{r}) between G_{Lmax} and L_{max} greater than 1.55 (Fig. 6b) was approximately 35,000, which were excluded from histogram statistics because there was a high probability that the length of at least one of the two datasets was erroneous. The peak value of the histogram (Fig. 6b) of R_{r} is in the interval 1.05–1.15 and R_{r} in the interval 0.95–1.25 accounts for 64.55%. The glacier length G_{Lmax} in this study was generally longer than L_{max} and the average value was approximately 10%, which indicates that glacier centerline lengths were probably underestimated in previous studies. In addition, the abnormal value of the length ratio of glacier L_1 was the highest and the median value was high (Fig. 6c). The R_{r} values of glaciers L_4–L_{10} fluctuated greatly. The R_{r} distributions of glaciers L_2 and L_3 were relatively concentrated. The reason for this is that the length of glacier L_1 was affected by the DEM, while glaciers L_4–L_{10} were mainly disturbed by differences in glacier scale and the accuracy of the auxiliary line.

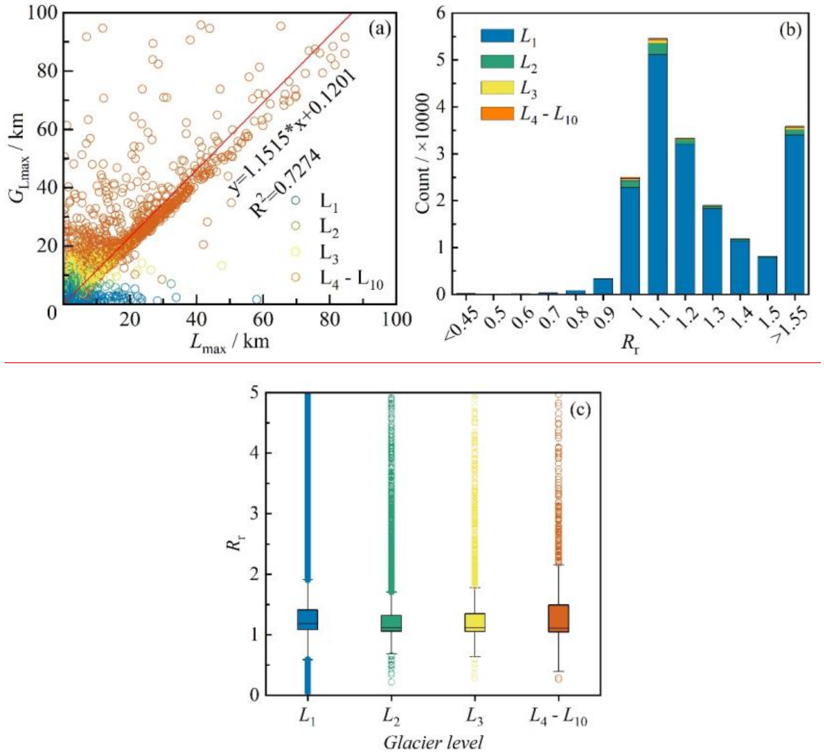

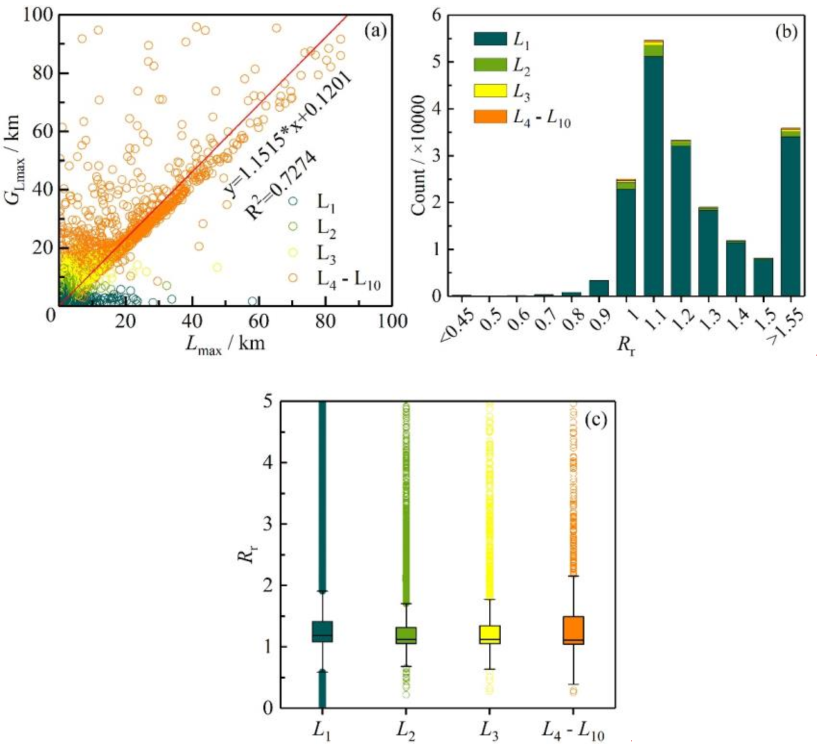

Figure 6. Comparison of longest centerlines calculated in this study and by Machguth and Huss (2014). **(a)** Linear regression of maximum length for all input glaciers (*IGODS*), determined in the G_{Lmax}, calculated in this study and $L_{\max}$ obtained in Machguth and Huss (2014). **(b)** Histogram of length ratio (R_{r}, $G_{\mathrm{Lmax}}/L_{\max}$) for distinct grades of glaciers. **(c)** Box plots of length ratio (R_{r}) for different scales of glaciers.

Comparisons between G_{Lmax} and $L_{\max}$ for each first-order glacier region and all random samples are shown in Appendix B. There was a preferable fitting degree between G_{Lmax} and $L_{\max}$ in seven glacier regions including R01, R04, R07, and R12–R15, in which the R^2 was larger than 0.95 (Fig. B1). The R_{r} in R17 ($R^2 = 0.8174$), R05 ($R^2 =$ 0. 8136), and R03 ($R^2 = 0.6311$) were poor, whereas that in R19 ($R^2 = 0.5487$) was the worst. The R^2 values of the other eight glacier regions were between 0.85 and 0.95. The histograms (Fig. B2) suggest that G_{Lmax} and $L_{\max}$ fitted well in R04, R06, R07, R09, and R12–R15 because they had recognizable single peak values. The peak values of R03, R05, R17, and R19 were not prominent and the proportion of glaciers with $R_{\mathrm{r}} > 1.55$ was extremely high, further increasing the uncertainty in glacier length results in these four regions. R01, R07, R08, R11–R15, and R18 performed well in the box plot (Fig. B3), whereas the results for R09 were not good. Moreover, the fitting degree of all random samples was poor (Fig. B1, $R^2 = 0.7547$), the peak value was more prominent (Fig. B2), and the length ratio distribution of glaciers of different grades was relatively scattered (Fig. B3). In general, the glacier lengths of R07 and R12–R15 were the closest, while there were significant differences in R03, R05, R17, and R19.

Furthermore, graphic results collected for the maximum length of glaciers in parts of High Asia (Machguth and Huss, 2014) were used to compare the results. In two parts of R15, Mount Qomolangma and its surrounding area (Fig. 7a) and Kangchenjunga and its surrounding area (Fig. 7b), the glaciers showed a flaky distribution for mapping. Visible comparison was suggested that the extraction method used in this study had likely a strong ability to obtain the maximum length of glaciers (Fig. 7a) and that its sensitivity to topography was lower than that of Machguth and Huss (2014) (Fig. 7b). Both sets of glacier length extraction schemes were valid and there were large differences only in a few glaciers or in certain types of glaciers, such as slope glaciers and ice caps.

~~Note that the comparative analysis results of the two lengths were relative, random samples were limited, and it was difficult to accurately reflect the quality of the dataset in this study. Owing to these limitations, the quality of the data must be determined again by secondary evaluation before applying to specific regions. Additionally, the automatic extraction algorithm in this study is more suitable for application to single-outlet glaciers, particularly valley glaciers; it is not suitable for ice caps, flat-top glaciers, and tidal glaciers that are widely distributed in the Antarctic, sub-Antarctic, northern Canadian Arctic, and other areas. Even if our algorithm can produce promising results, accuracy remains a concern.~~

4.2.3 Uncertainties and possibilities for improvement

Although we compared the two current global length datasets, it is still difficult to accurately reflect the quality of the dataset in this study. For some glaciers that are not provided centerlines in this dataset, data users need to update the corresponding glacier outlines and could use the automatic extraction tool provided in this study to generate their centerlines, which involves the defective glacier outlines (*FGODS*), nominal glaciers and ice caps of the RGI v6.0. Specifically, the centerlines of the *FGODS* rely on the glacier outlines that meet the requirements of this study. These glacier outlines include glacier inventory data from other sources, or the *FGODS* that are repaired by some algorithms or manual process. Nominal glaciers are similar to *FGODS*, and also require users to obtain corresponding glacier outlines. Automatic approaches dividing ice caps from glacial complexes into individual glaciers are currently limited, and data users can only use their own criterion to divide ice caps and then use our tool to generate centerlines. In addition, prioritizing the coverage of this dataset, we designed a geometry-based algorithm to repair FGODS and provided data users with their centerlines in the form of supplementary dataset, and corresponding codes and results can be seen in sub-datasets *CODES* and *SUP_220707*.

The automatic extraction algorithm in this study is more suitable for application to single-outlet glaciers, particularly valley glaciers; it is not suitable for ice caps, flat-top glaciers, and tidal glaciers that are widely distributed in the Antarctic, sub-Antarctic, northern Canadian Arctic, and other areas. In short, the uncertainties in this dataset come probably from the centerlines of some slope glaciers and the ice caps that are not identified in RGI v6.0, or a few centerlines with unpredictable quality due to the input data such as the incorrect glacier polygons, erroneous DEMs. In future work, better glacier inventory and more accurate DEM are useful for the improvement of centerline quality. On the other hand, optimizing the automatic glacier segmentation approach, DEM-based extraction algorithm of glacier feature lines and centerline trade-off algorithm are also probable ways to further improve the accuracy of glacier centerlines. In addition, it is probably beneficial to further clarify the type of each glacier in the glacier inventory for the estimates of centerline accuracy.

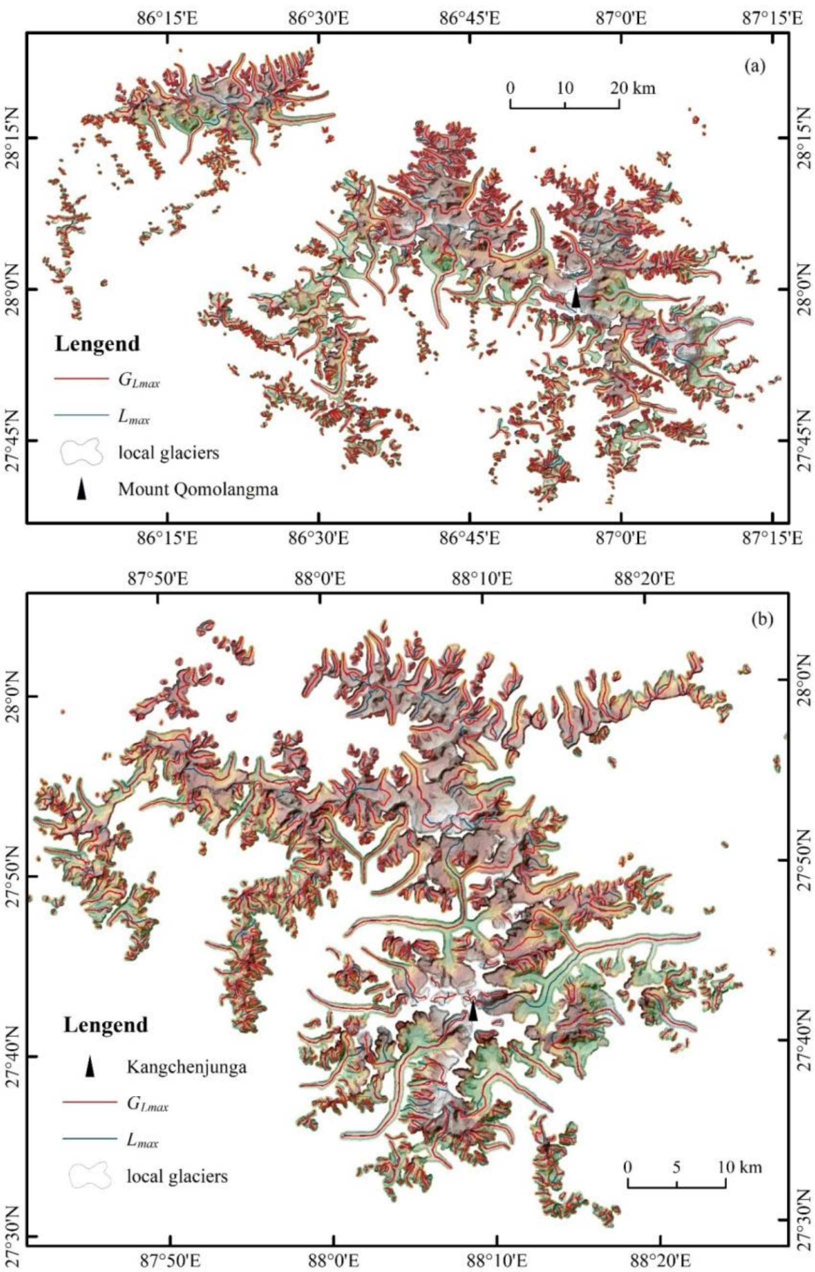

Figure 7. Visible comparison of the longest center lines calculated in this study and by Machguth and Huss (2014). The figure shows two glacier-covered regions in the Himalayas, covering Mount Qomolangma (**panel a**) and Kangchenjunga (**panel b**, the world's third highest mountain) and their surrounding areas. The background is the DEM used for the calculation.

5 Data availability

Global glacier centerline dataset (*GGCLDS*), global glacier maximum length dataset (*GGMLDS*), and other relevant datasets are available at https://doi.org/10.11922/sciencedb.01643 (Zhang and Zhang, 2022)~~ (or https://www.scidb.cn/en/s/BRzaUf)~~. All ~~14~~ 17 sub-datasets of this dataset are listed in Table 5.

Table 5. Description of the members contained in this dataset.

Acronym	Data format	Data volume	Description
IGODS	*.shp	316 MB	Input glacier outline dataset
GGEDS	*.tif	3.70 GB	Global glacier elevation dataset
GGCLDS		838 MB	Global glacier centerline dataset
GGMLDS		616 MB	Global glacier maximum length dataset
GACLDS		302 MB	Global glacier accumulation region length dataset
GABLDS		358 MB	Global glacier ablation region length dataset
GOSRDS		1.16 GB	Global glacier outline segmentation result dataset
GLHPDS		11 MB	Global glacial local highest point dataset
GLPDS	*.shp	6.25 MB	Global glacial lowest point dataset
GUGODS		3.95 MB	Unsuccessful global glacier outline dataset
FGODS		119 MB	Global flawed glacier outline dataset
GGECDS		334 MB	Global glacier external contour dataset
GGBMDS		374 MB	Global glacier buffer mask dataset
MHMLDS		8.32 MB	The maximum length of Machguth and Huss in High Asia
SUP_220~~628~~707		681 MB	Updated the centerlines of the repaired *FGODS*
CODES	*.py	40~~.5~~ KB	Related codes of data process in bulk
LOGS	*.txt	1.27 MB	Related logfiles of data process in bulk

6 Conclusions

In this study, a new dataset on the centerline of global glaciers was constructed and the maximum length was calculated based on the global glacier inventory (RGI v6.0) and global glacier region DEM (*GGEDS*, composed of NASADEM, ASTER GDEM v3, and Copernicus DEM). In total, 198,137 glacier centerlines were generated, accounting for 99.74% of the total number of imported glaciers (*IGODS*) and 91.52% of the total number of the global glacier inventory. The comprehensive extraction accuracy of these glacier centerlines (*GGCLDS*) used in random self-assessment was 89.68%. The glacier length (G_{Lmax}) obtained in this study was generally approximately 10% longer than that of L_{max} on average. Nevertheless, our method showed a stronger ability to obtain the maximum length, and we believe that the resulting errors were controllable. Furthermore, the preprocessing algorithm we designed accurately identified 10,764 erroneous glacier polygons from RGI v6.0, which formed the defective glacier dataset (*FGODS*).

A dataset containing ~~14~~ 17 sub-datasets was generated through the above work, including two basic input datasets (*IGODS* and *GGEDS*), two key result datasets (*GGCLDS* and *GGMLDS*), four process datasets, ~~and~~ six derived result datasets, and three supplementary datasets. Ice caps, nominal glaciers, and erroneous glacier polygons were eliminated from most sub-datasets in this study, accounting for approximately 8.25% of the total RGI v6.0. The poor status of these glacier polygons was not sufficient to support the automatic extraction of glacier centerlines, which needs to be improved in future work. Inevitably, there were some defects in the algorithm or datasets that need to be considered in future research. For instance, the glacial regions (R19 and R03) with the worst results were added to the dataset to prioritize data coverage integrity. It is worth noting that the global glacier DEM dataset (*GGEDS*), global glacier external outline dataset (*GGECDS*), and global glacier buffer mask datasets (*GGBMDS*) cover all glaciers in RGI v6.0. Accordingly, they will help researchers design more efficient automated extraction algorithms to produce datasets containing all types of glacier centerlines and lengths worldwide, which is our next goal.

Appendix A: Model parameters resulting from the Central Asia Glacier and extended to worldwide calculations are listed in Table A1.

Table A1. Parameterization scheme for extracting global glacier centerlines.

Par.	Description	Value (Levels 1-10)	Unit
P_1	Maximum distance between adjacent vertexes	10	m
P_2	Buffer distance outside the glacier outline	30	m
P_3	Threshold of accumulative flow	5 - 8, 10, 20, 30, 50, 100, 200	int × 10^3
P_4	Length of the shortest auxiliary line	10 - 19	int
P_5	Length of the longest auxiliary line	2 - 11	int
P_6	Interval for searching the local highest points	50, 60, 70, 80, 90,100, 200, 300, 400, 500	count
P_7	Matching tolerance of the vertexes of polyline	0.2 ,0.2 ,0.5 ,0.5 ,1 (L_5 - L_{10})	m
P_8	Size of grid cell in Euclidean allocation	1, 5, 15, 15, 30 (L_5 - L_{10})	m
P_9	Minimum distance between the adjacent $P_{\max}$	10, 15, 30, 60, 120, 150, 200, 300, 400, 500	count
P_{10}	Smoothing tolerance of polylines	5, 10, 15, 20, 30 (L_5 - L_{10})	m
P_{11}	Length threshold of the longest auxiliary line	10190	km^2

Notes: The calculation method for each parameter is detailed in Zhang et al. (2021). $P_{\max}$ and L refer to the local highest points and grades of the glacier, respectively.

Appendix B: Comparison of longest centerlines calculated in this study and by Machguth and Huss (2014) for all samples and the different first-order glacier regions of RGI v6.0. Linear regression of the two lengths, histogram of length ratio (R_r), and box plots of R_r for glaciers of different grades in these regions were in Figure B1, B2, and B3, respectively.

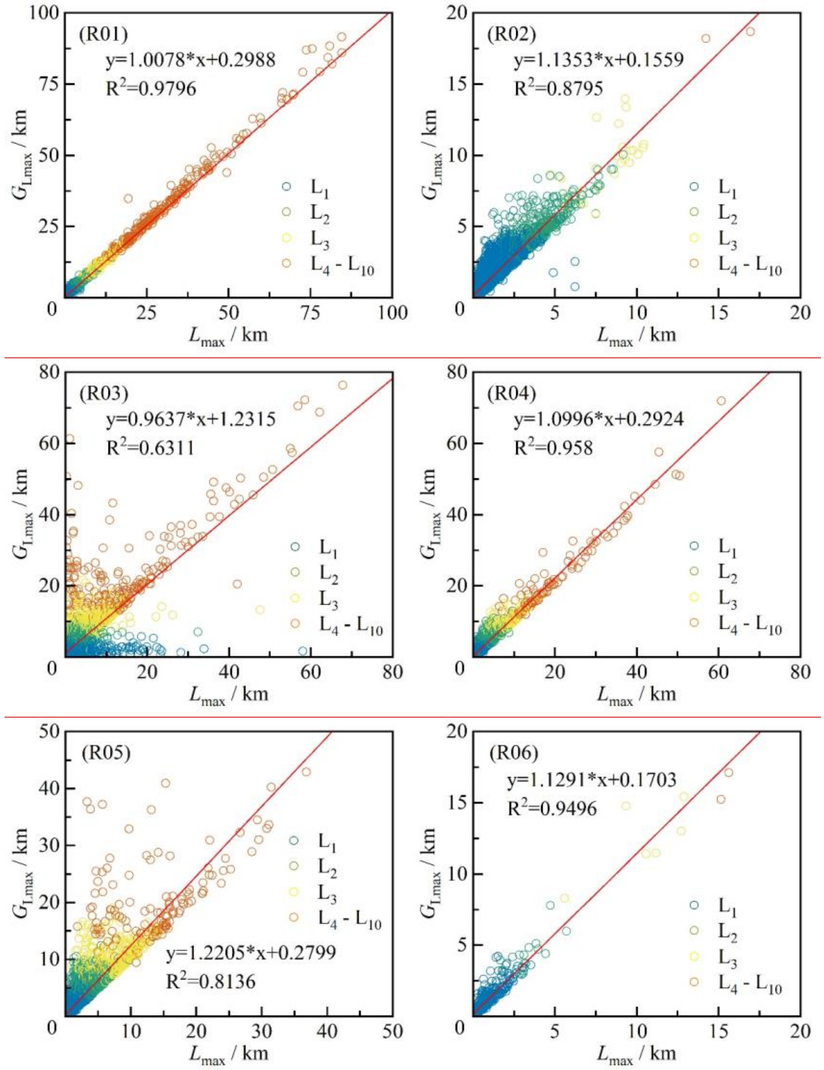
(R01)
y=1.0078*x+0.2988
R^2=0.9796
(R02)
y=1.1353*x+0.1559
R^2=0.8795
(R03)
y=0.9637*x+1.2315
R^2=0.6311
(R04)
y=1.0996*x+0.2924
R^2=0.958
(R05)
y=1.2205*x+0.2799
R^2=0.8136
(R06)
y=1.1291*x+0.1703
R^2=0.9496
L1
L2
L3
L4 - L10
G_L,max / km
L_max / km

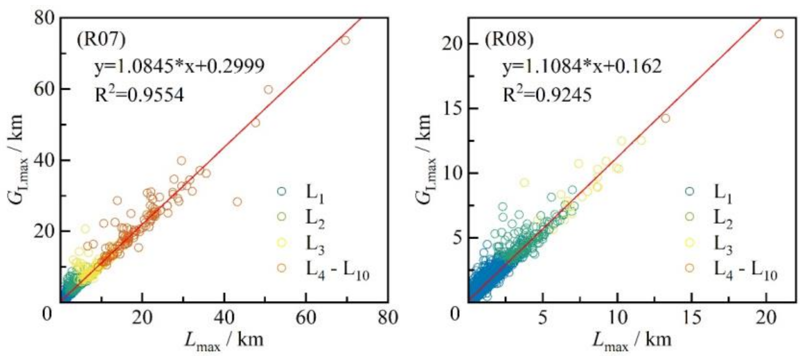

(R07)
y=1.0845*x+0.2999
R2=0.9554
L1
L2
L3
L4 - L10
GLmax / km
Lmax / km
(R08)
y=1.1084*x+0.162
R2=0.9245
L1
L2
L3
L4 - L10
GLmax / km
Lmax / km

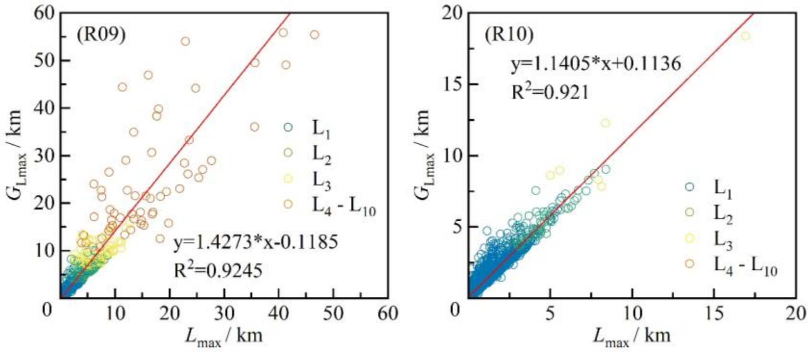

(R09)
y=1.4273*x-0.1185
R2=0.9245
L1
L2
L3
L4 - L10
GLmax / km
Lmax / km
(R10)
y=1.1405*x+0.1136
R2=0.921
L1
L2
L3
L4 - L10
GLmax / km
Lmax / km

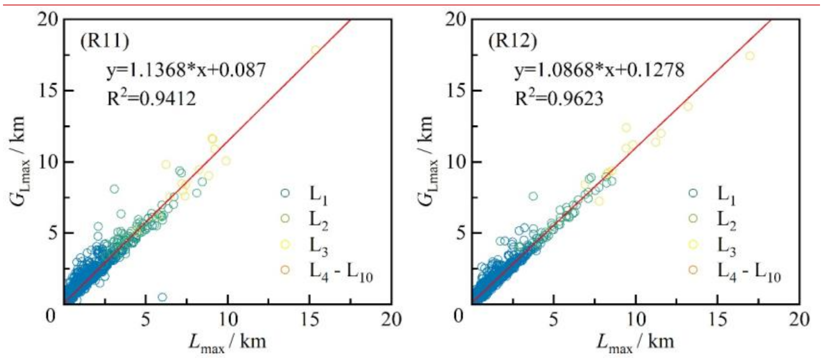

(R11)
y=1.1368*x+0.087
R2=0.9412
L1
L2
L3
L4 - L10
GLmax / km
Lmax / km
(R12)
y=1.0868*x+0.1278
R2=0.9623
L1
L2
L3
L4 - L10
GLmax / km
Lmax / km

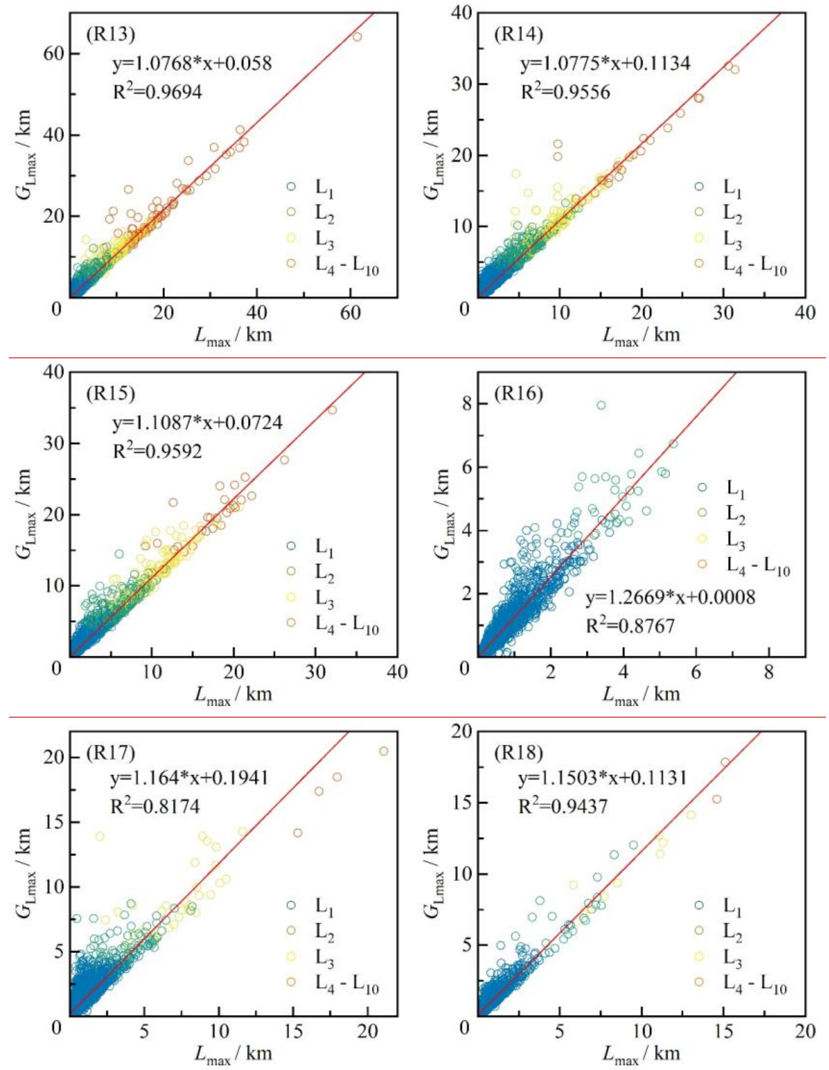
(R13)
y=1.0768*x+0.058
R^2=0.9694
(R14)
y=1.0775*x+0.1134
R^2=0.9556
(R15)
y=1.1087*x+0.0724
R^2=0.9592
(R16)
y=1.2669*x+0.0008
R^2=0.8767
(R17)
y=1.164*x+0.1941
R^2=0.8174
(R18)
y=1.1503*x+0.1131
R^2=0.9437
L_1
L_2
L_3
L_4 - L_{10}
G_{Lmax} / km
$L_{\max}$ / km

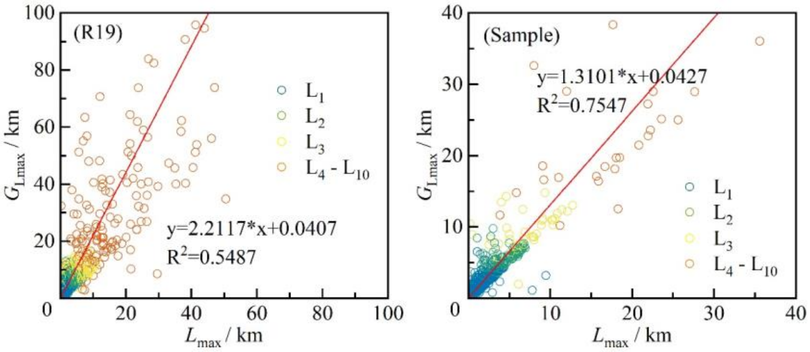
(R19)
y=2.2117*x+0.0407
R2=0.5487
L1
L2
L3
L4 - L10
GL,max / km
Lmax / km
(Sample)
y=1.3101*x+0.0427
R2=0.7547

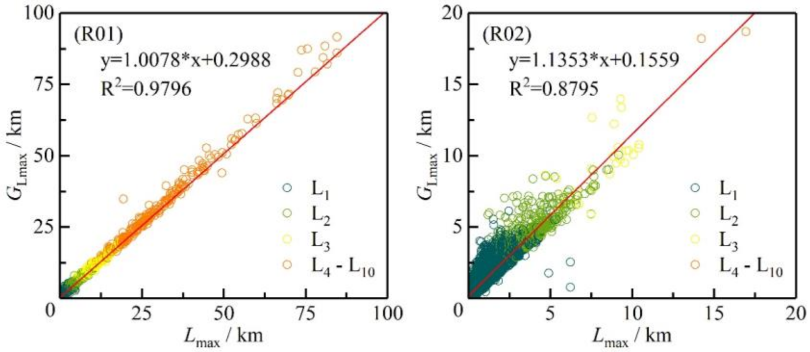
(R01)
y=1.0078*x+0.2988
R2=0.9796
L1
L2
L3
L4 - L10
GL,max / km
Lmax / km
(R02)
y=1.1353*x+0.1559
R2=0.8795

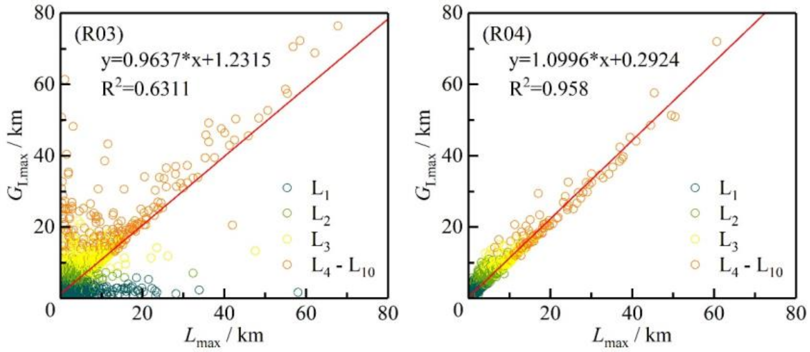
(R03)
y=0.9637*x+1.2315
R2=0.6311
L1
L2
L3
L4 - L10
GL,max / km
Lmax / km
(R04)
y=1.0996*x+0.2924
R2=0.958

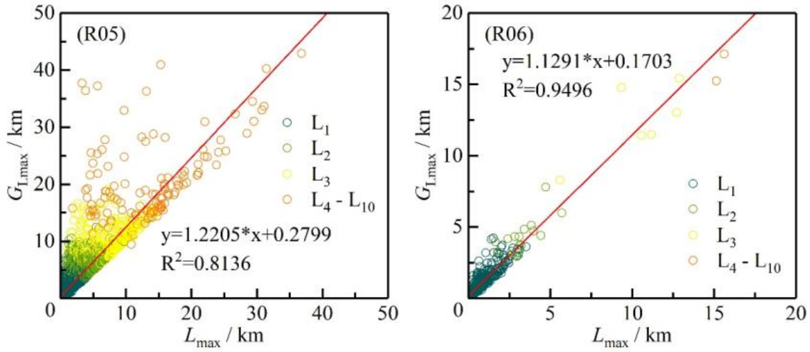
(R05)
y=1.2205*x+0.2799
R2=0.8136
L1
L2
L3
L4 - L10
GL,max / km
Lmax / km
(R06)
y=1.1291*x+0.1703
R2=0.9496

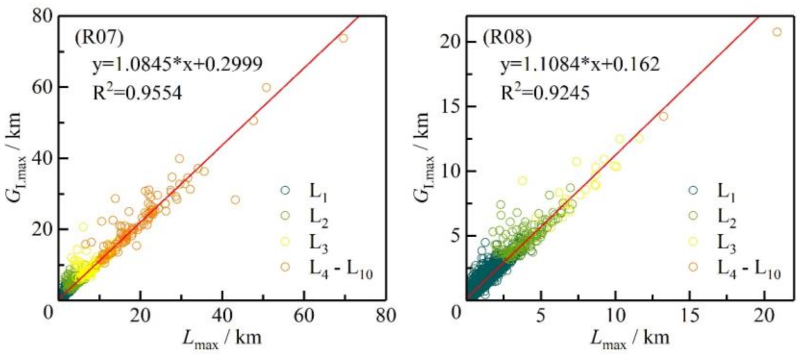

(R07)
y=1.0845*x+0.2999
R^2=0.9554
G_{Lmax} / km
$L_{\max}$ / km
L_1
L_2
L_3
L_4 - L_{10}
(R08)
y=1.1084*x+0.162
R^2=0.9245
G_{Lmax} / km
$L_{\max}$ / km
L_1
L_2
L_3
L_4 - L_{10}

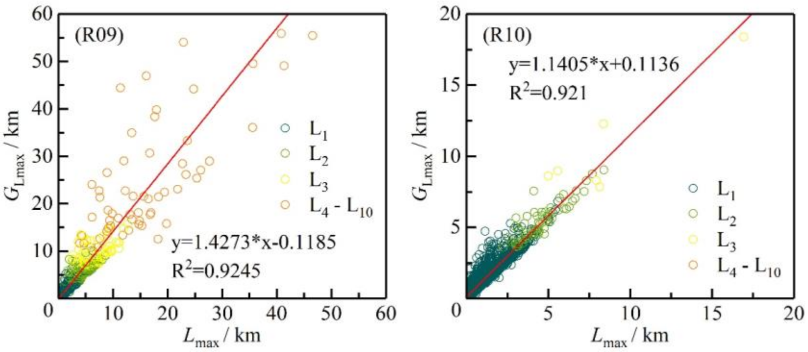

(R09)
y=1.4273*x-0.1185
R^2=0.9245
G_{Lmax} / km
$L_{\max}$ / km
L_1
L_2
L_3
L_4 - L_{10}
(R10)
y=1.1405*x+0.1136
R^2=0.921
G_{Lmax} / km
$L_{\max}$ / km
L_1
L_2
L_3
L_4 - L_{10}

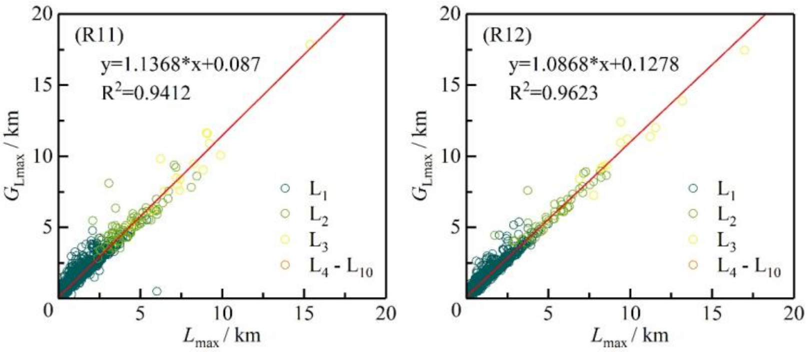

(R11)
y=1.1368*x+0.087
R^2=0.9412
G_{Lmax} / km
$L_{\max}$ / km
L_1
L_2
L_3
L_4 - L_{10}
(R12)
y=1.0868*x+0.1278
R^2=0.9623
G_{Lmax} / km
$L_{\max}$ / km
L_1
L_2
L_3
L_4 - L_{10}

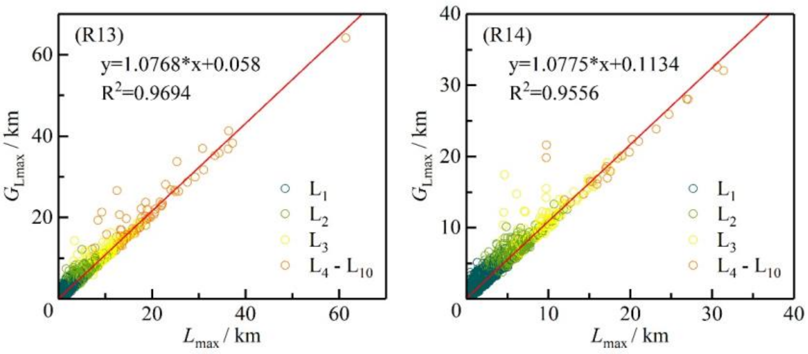

(R13)
y=1.0768*x+0.058
R^2=0.9694
G_{Lmax} / km
$L_{\max}$ / km
L_1
L_2
L_3
L_4 - L_{10}
(R14)
y=1.0775*x+0.1134
R^2=0.9556
G_{Lmax} / km
$L_{\max}$ / km
L_1
L_2
L_3
L_4 - L_{10}

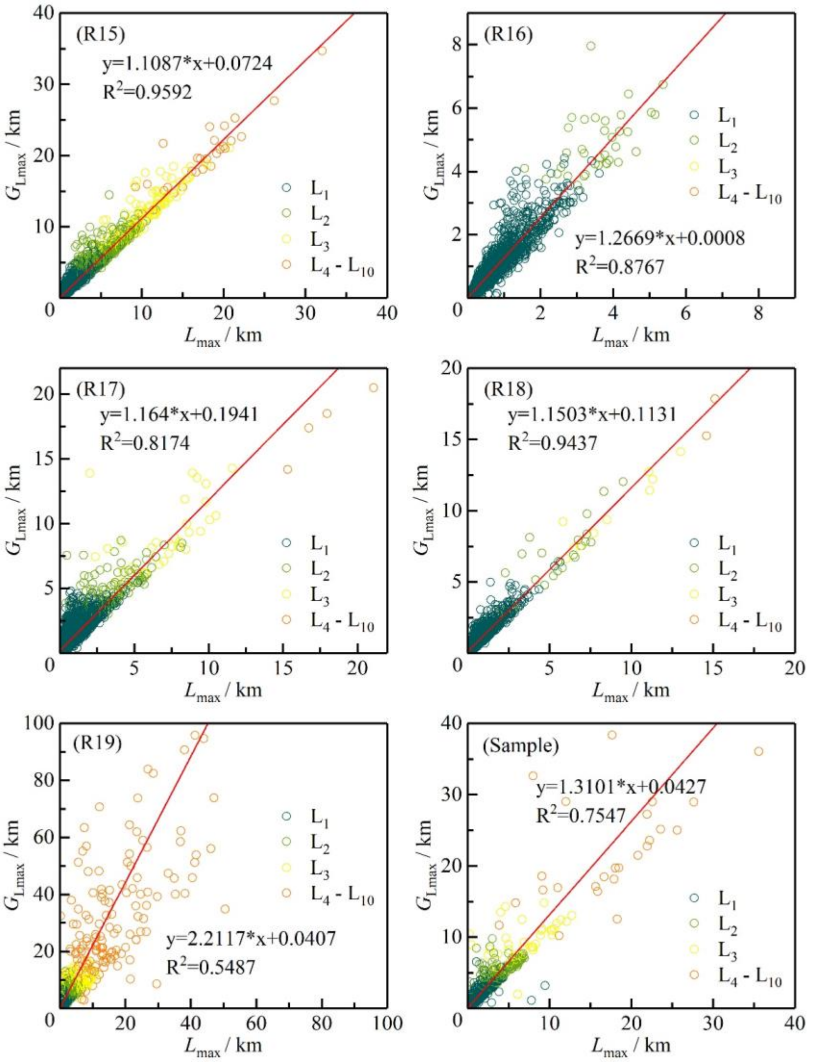

Figure B1. Linear regression in different glacier regions between glacier length (G_{Lmax}) calculated in this study and glacier length (L_{max}) calculated by Machguth and Huss (2014).

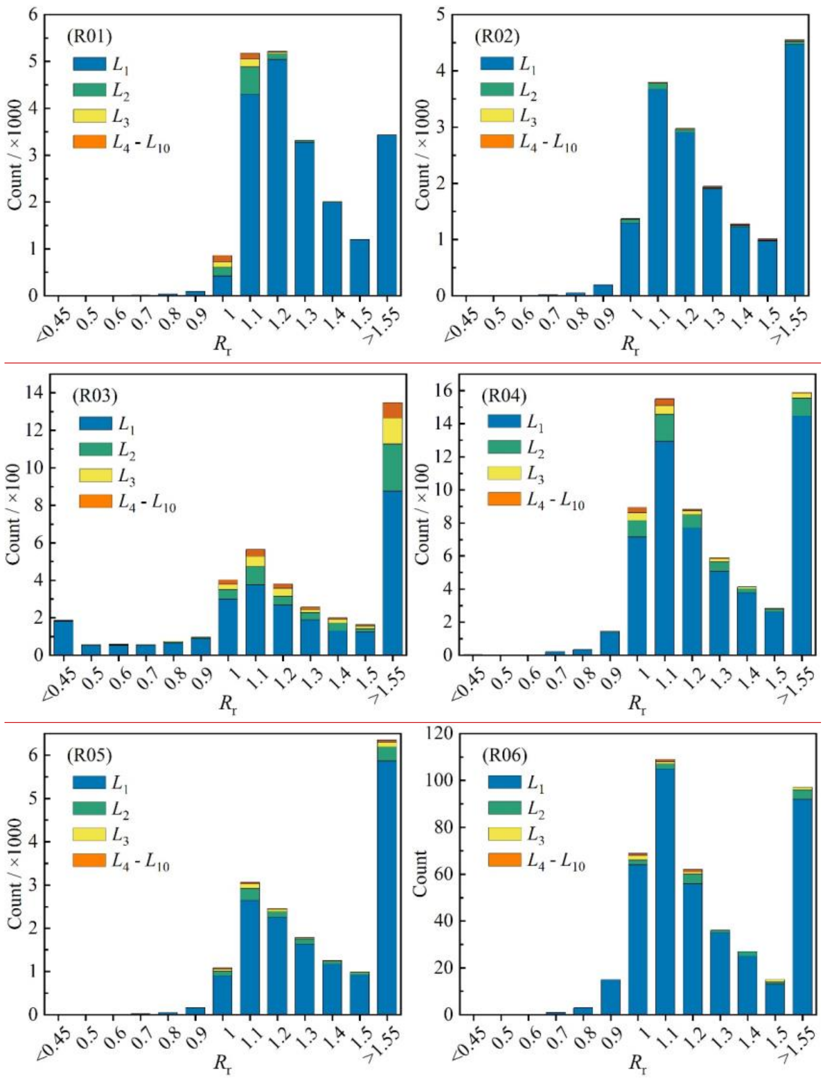

(R01)
(R02)
(R03)
(R04)
(R05)
(R06)
L_1
L_2
L_3
L_4 - L_{10}
Count / ×1000
Count / ×100
Count
R_r
<0.45 0.5 0.6 0.7 0.8 0.9 1 1.1 1.2 1.3 1.4 1.5 >1.55

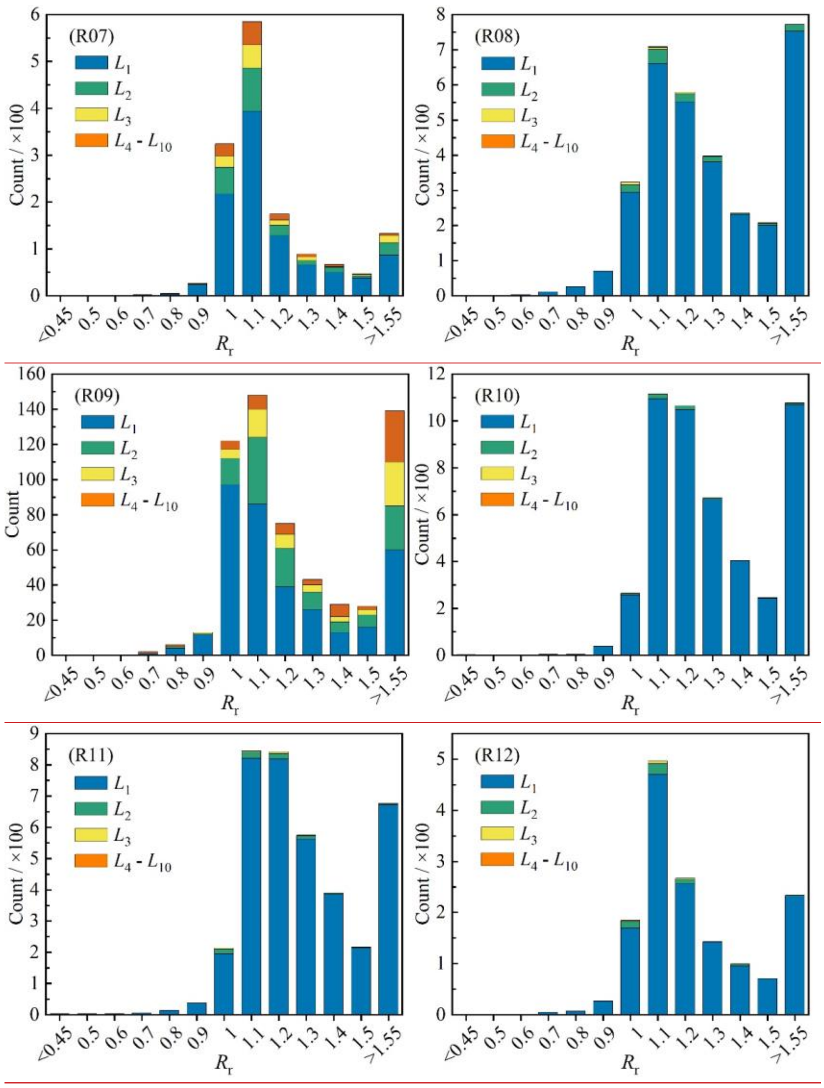
(R07)
(R08)
(R09)
(R10)
(R11)
(R12)
L_1
L_2
L_3
L_4 - L_{10}
Count / ×100
Count
R_r
<0.45
0.5
0.6
0.7
0.8
0.9
1
1.1
1.2
1.3
1.4
1.5
>1.55

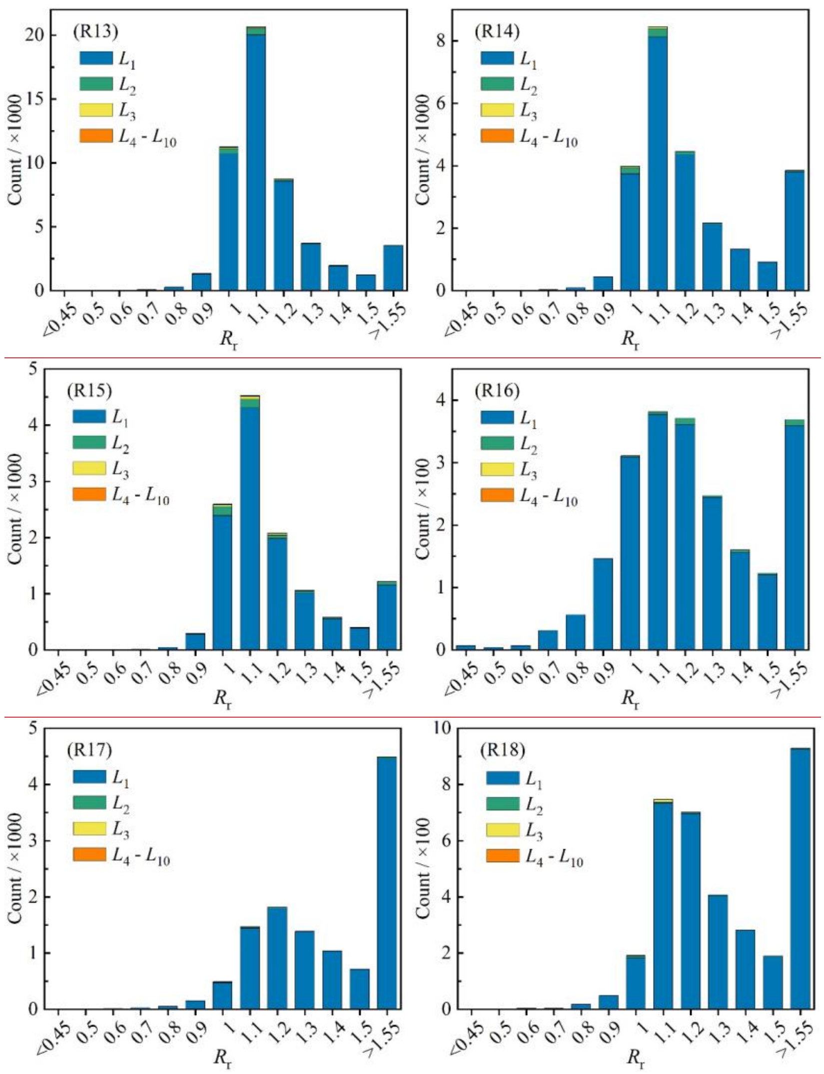
(R13)
(R14)
(R15)
(R16)
(R17)
(R18)
L_1
L_2
L_3
L_4 - L_{10}
Count / ×1000
Count / ×100
R_r
<0.45
0.5
0.6
0.7
0.8
0.9
1
1.1
1.2
1.3
1.4
1.5
>1.55

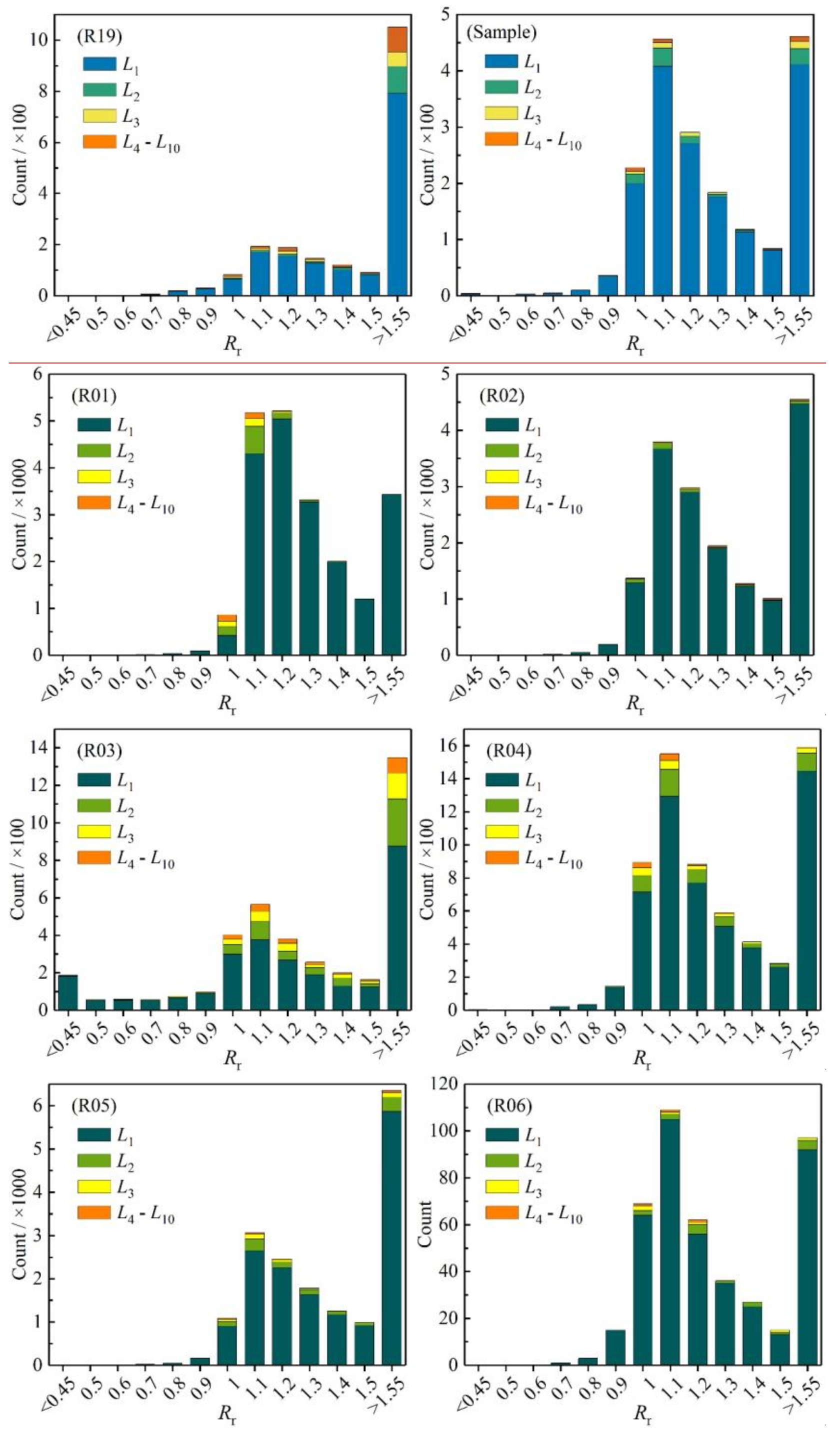
(R19)
(Sample)
(R01)
(R02)
(R03)
(R04)
(R05)
(R06)
L_1
L_2
L_3
L_4 - L_{10}
Count / ×100
Count / ×1000
Count
R_r
<0.45
0.5
0.6
0.7
0.8
0.9
1
1.1
1.2
1.3
1.4
1.5
>1.55

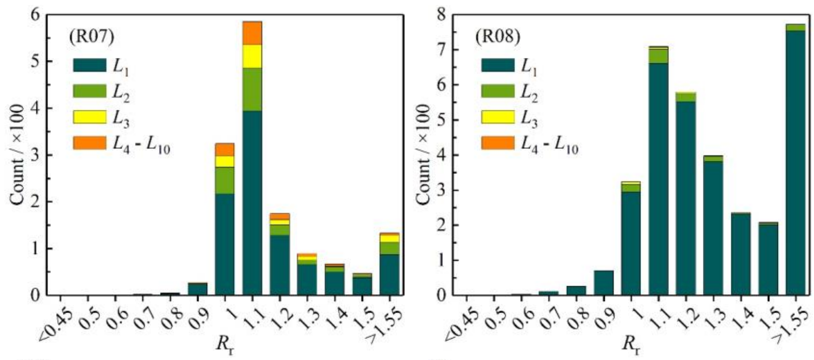
(R07)
(R08)
L_1
L_2
L_3
L_4 - L_{10}
Count / ×100
R_r

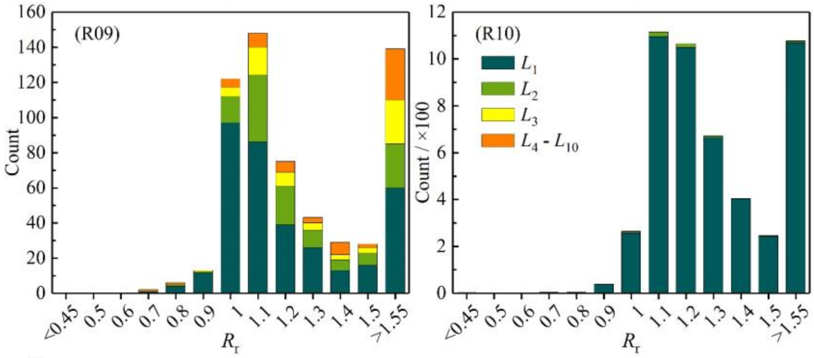
(R09)
(R10)
L_1
L_2
L_3
L_4 - L_{10}
Count
Count / ×100
R_r

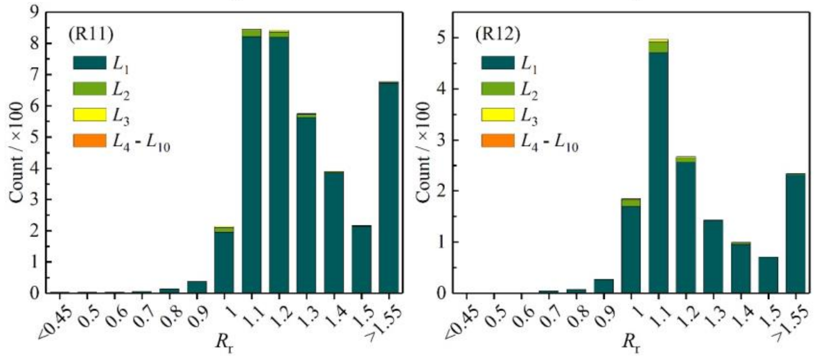
(R11)
(R12)
L_1
L_2
L_3
L_4 - L_{10}
Count / ×100
R_r

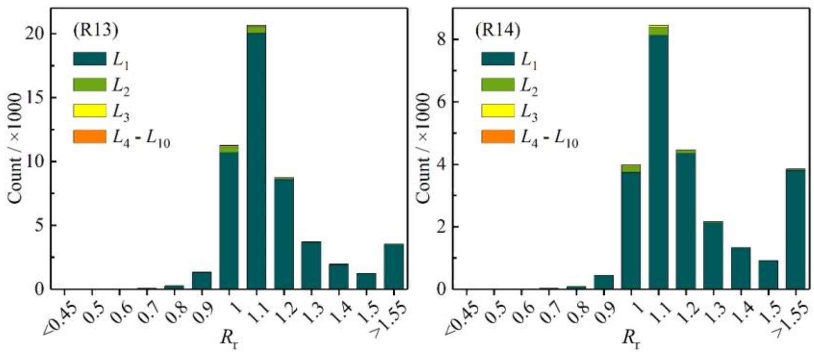
(R13)
(R14)
L_1
L_2
L_3
L_4 - L_{10}
Count / ×1000
R_r

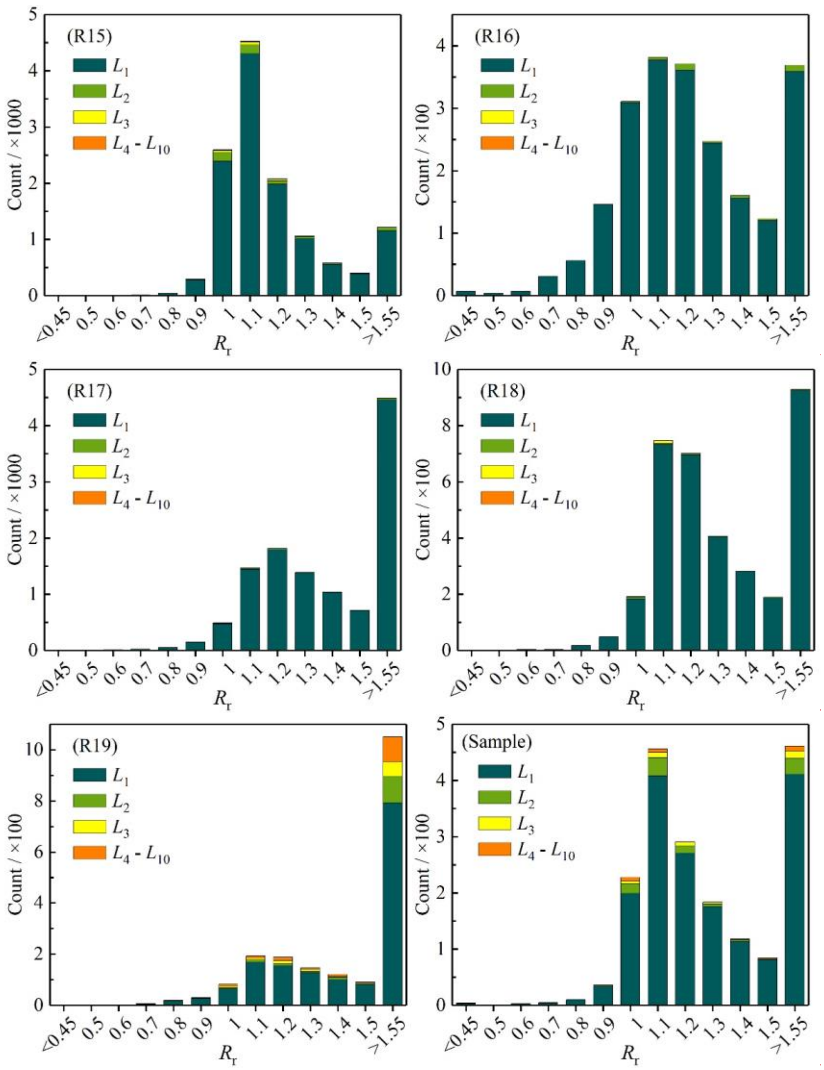

Figure B2. Histograms of the length ratio (R_r, G_{Lmax}/L_{max}) of distinct glacier grades in glacier-covered regions and all samples.

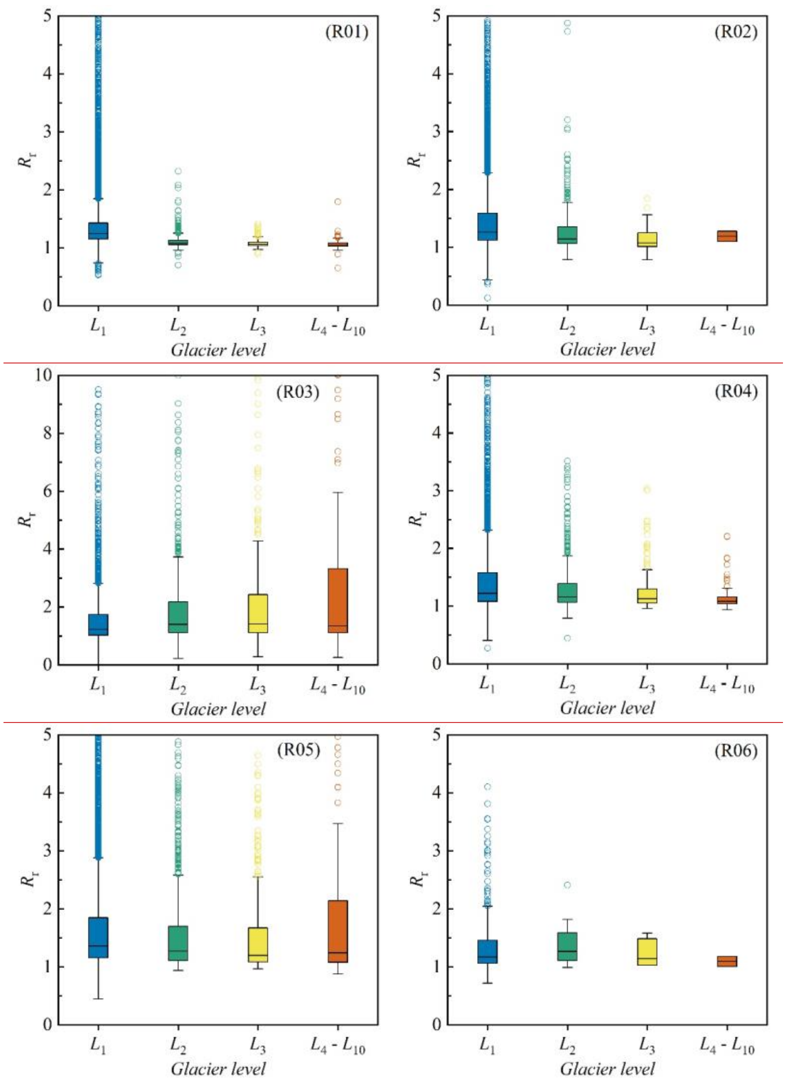
(R01)
(R02)
(R03)
(R04)
(R05)
(R06)
R_r
L_1
L_2
L_3
L_4 - L_{10}
Glacier level

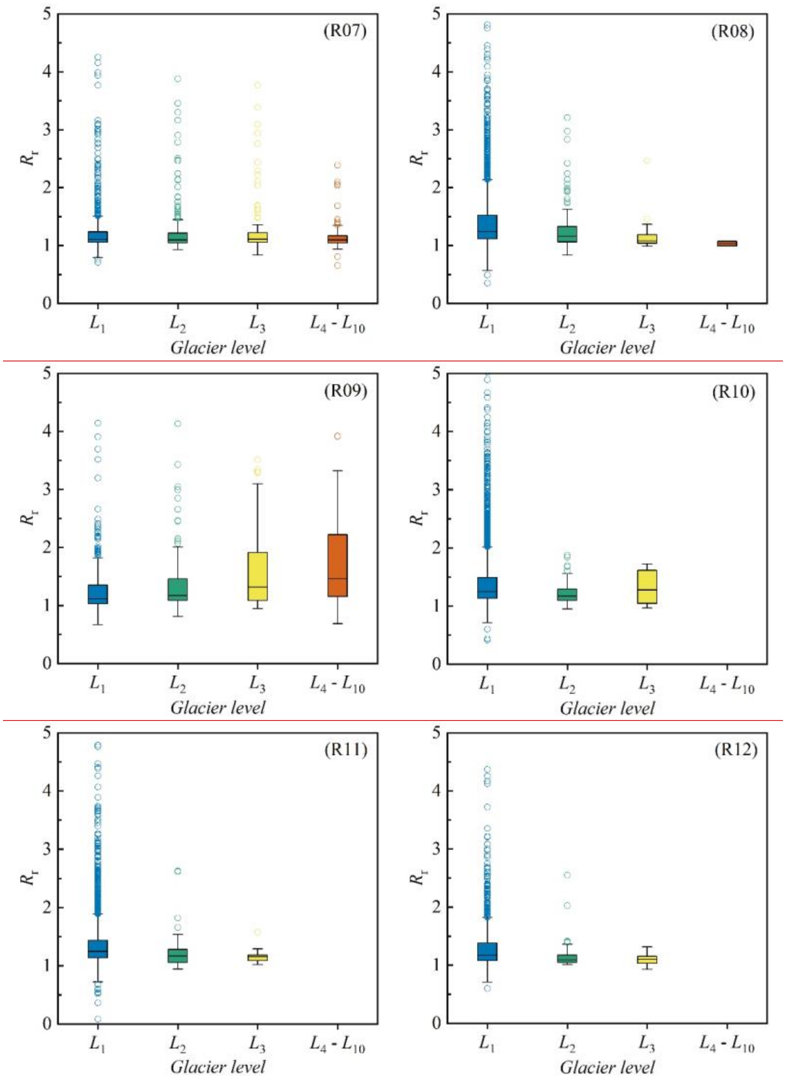
(R07)
(R08)
(R09)
(R10)
(R11)
(R12)
R_r
L_1
L_2
L_3
L_4 - L_{10}
Glacier level

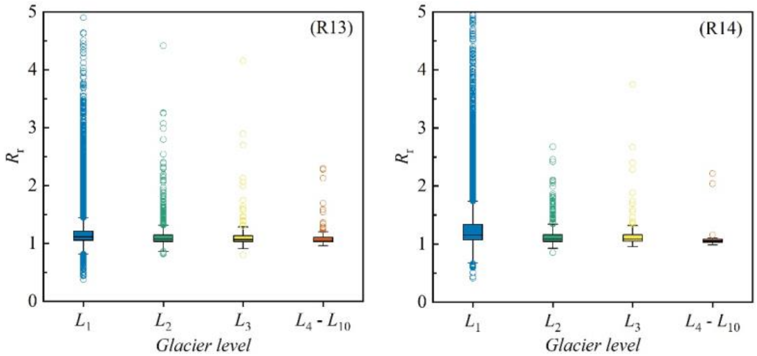
(R13)
(R14)
R_r
0
1
2
3
4
5
L_1
L_2
L_3
L_4 - L_{10}
Glacier level

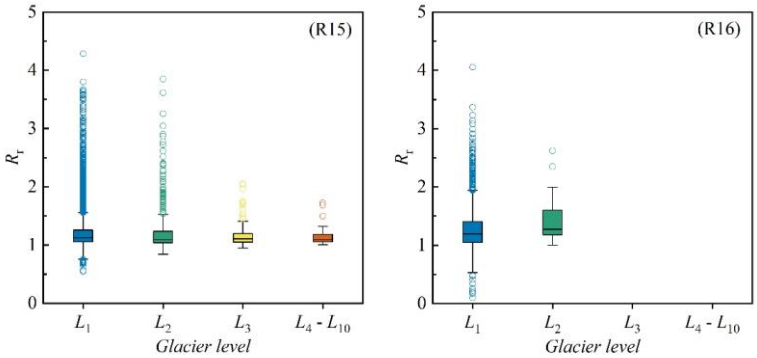
(R15)
(R16)
R_r
0
1
2
3
4
5
L_1
L_2
L_3
L_4 - L_{10}
Glacier level

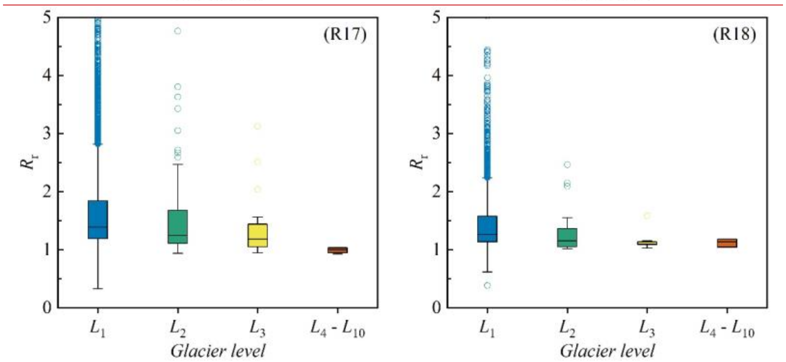
(R17)
(R18)
R_r
0
1
2
3
4
5
L_1
L_2
L_3
L_4 - L_{10}
Glacier level

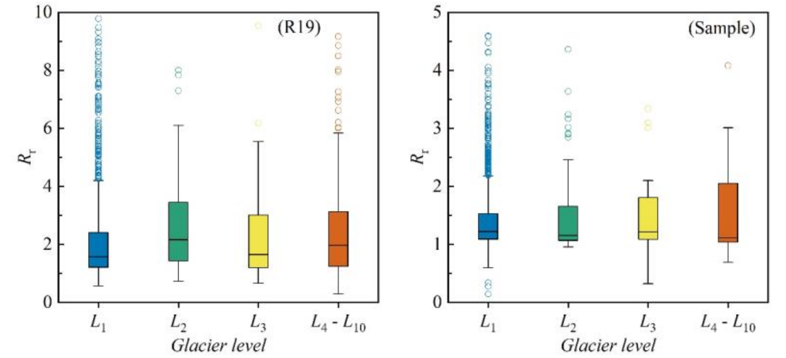
(R19)
(Sample)
R_r
L_1
L_2
L_3
L_4 - L_{10}
Glacier level

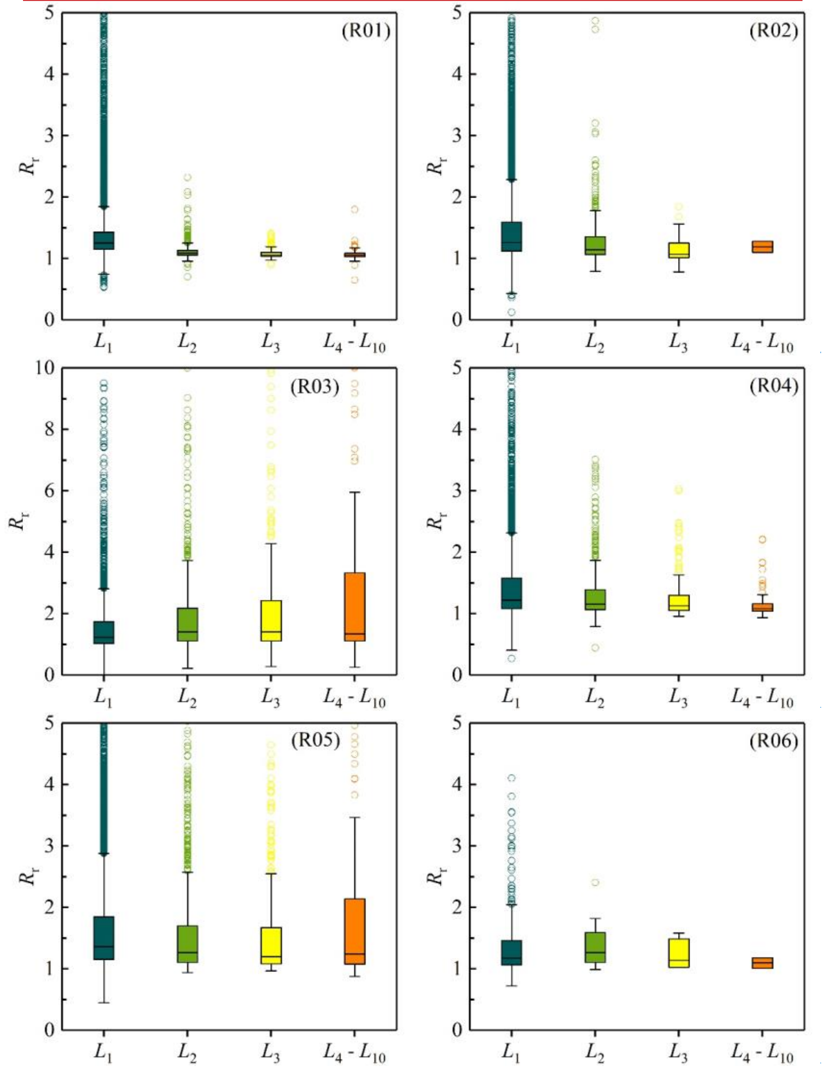
(R01)
(R02)
(R03)
(R04)
(R05)
(R06)
R_r
L_1
L_2
L_3
L_4 - L_{10}

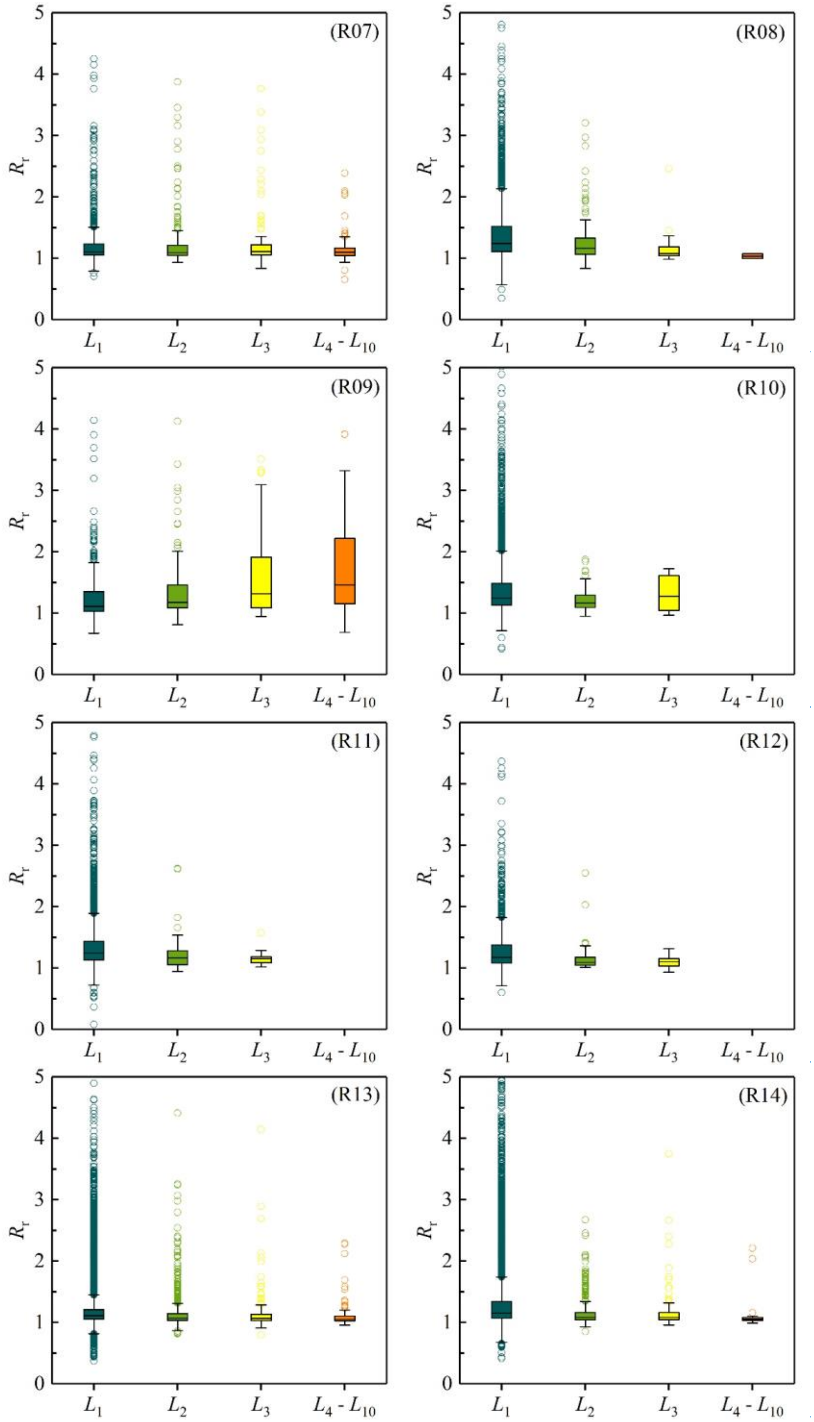
(R07)
(R08)
(R09)
(R10)
(R11)
(R12)
(R13)
(R14)
R_r
L_1
L_2
L_3
L_4 - L_{10}

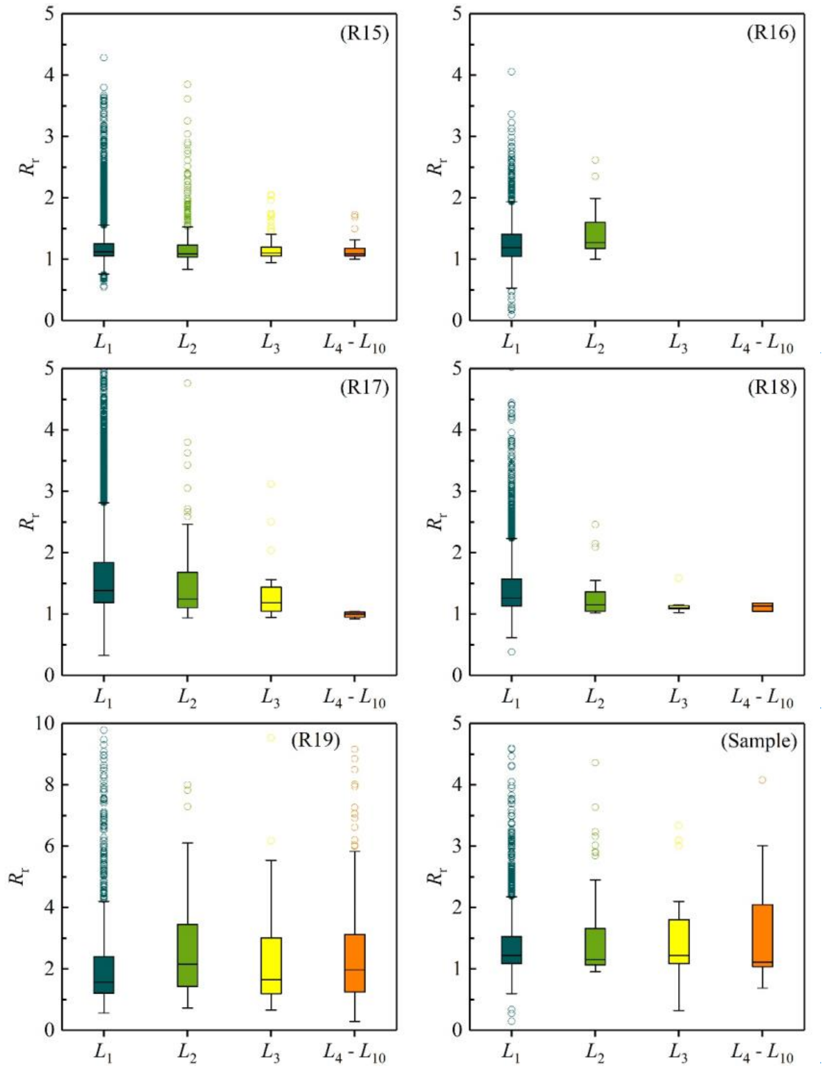

Figure B3. Box plots of length ratio (R_r, $G_{\mathrm{Lmax}}/L_{\mathrm{max}}$) of glaciers of distinct grades in every glacier-covered region and whole sample.

Supplement.

The Supplement consists of two parts: (1) 'GlacierCenterlines_Py27' (version 5.2.1), the updated automatic extraction tool of glacier centerlines in this study, which fixed some defects compared with version 5.2.0 (https://doi.org/10.5194/tc-151955-2021-supplement). (2) 'Other_parameters_T1.txt' is the parameter file for extracting the global glacier centerlines.

Author contributions.

All authors contributed to writing and editing the manuscript. DZ processed the data, performed all calculations, created all figures, and wrote most of the manuscript. SZ contributed significantly to the development of the analyses, figures, and writing. XY contributed to the development of the data production strategy and writing. GZ and WL contributed to the initial data production. SW participated in writing Chapter 4.

Competing interests.

The authors declare that they have no conflict of interest.

Acknowledgments.

We thank editors, two reviewers and community scholars for their valuable comments that improved the manuscript. The authors would especially like to thank GLIMS for releasing the RGI v6.0 (http://www.glims.org/RGI/randolph.html, last accessed: November 15, 2021), LP DAAC for releasing the NASADEM (https://lpdaac.usgs.gov/news/release-nasadem-data-products/, last accessed: November 17, 2021), METI and NASA for jointly releasing the ASTER GDEM v3 (https://lpdaac.usgs.gov/news/nasa-and-meti-release-aster-global-dem-version-3/, last accessed: November 17, 2021), and the European Space Agency (ESA) for providing the Copernicus DEM (https://spacedata.copernicus.eu/web/cscda/cop-dem-faq, last accessed: November 17, 2021). This work is not possible without the support of open-access data.

Financial support.

This research was funded by the Second Tibetan Plateau Scientific Expedition and Research Program (STEP) (grant number: 2019QZKK020109) and China National Natural Science Foundation (grant numbers: 41730751, 42171124).

References

Abrams, M., Crippen, R., and Fujisada, H.: ASTER Global Digital Elevation Model (GDEM) and ASTER Global Water Body Dataset (ASTWBD), Remote Sensing, 12, https://doi.org/10.3390/rs12071156, 2020.

Aciego, S. M., Stevenson, E. I., and Arendt, C. A.: Climate versus geological controls on glacial meltwater micronutrient production in southern Greenland, Earth and Planetary Science Letters, 424, 51-58, https://doi.org/10.1016/j.epsl.2015.05.017, 2015.

Carabajal, C. C. and Boy, J. P.: Evaluation of Aster Gdem V3 Using Icesat Laser Altimetry, ISPRS - International Archives of the Photogrammetry, Remote Sensing and Spatial Information Sciences, XLI-B4, 117-124, https://doi.org/10.5194/isprsarchives-XLI-B4-117-2016, 2016.

Carrera-Hernández, J. J.: Not all DEMs are equal: An evaluation of six globally available 30 m resolution DEMs with geodetic benchmarks and LiDAR in Mexico, Remote Sensing of Environment, 261,

https://doi.org/10.1016/j.rse.2021.112474, 2021.
Cazenave, A.: Global sea-level budget 1993–present, Earth System Science Data, 10, 1551-1590, https://doi.org/10.5194/essd-10-1551-2018, 2018.
Farinotti, D., Huss, M., Fürst, J. J., Landmann, J., Machguth, H., Maussion, F., and Pandit, A.: A consensus estimate for the ice thickness distribution of all glaciers on Earth, Nature Geoscience, 12, 168-173, https://doi.org/10.1038/s41561-019-0300-3, 2019.
Farr, T. G., Rosen, P. A., Caro, E., Crippen, R., Duren, R., Hensley, S., Kobrick, M., Paller, M., Rodriguez, E., Roth, L., Seal, D., Shaffer, S., Shimada, J., Umland, J., Werner, M., Oskin, M., Burbank, D., and Alsdorf, D.: The Shuttle Radar Topography Mission, Reviews of Geophysics, 45, 1-33, https://doi.org/10.1029/2005rg000183, 2007.
Gao, Y. P., Yao, X. J., Liu, S. Y., Qi, M. M., Gong, P., An, L. N., Li, X. F., and Duan, H. Y.: Methods and future trend of ice volume calculation of glacier, Arid Land Geography, 41, 1204-1213, https://doi.org/10.12118/j.issn.1000-6060.2018.06.08, 2018.
Hansen, K., Hasenstab, K., and Schwartzman, A.: Estimating Mountain Glacier Flowlines by Local Linear Regression Gradient Descent, IEEE Transactions on Geoscience and Remote Sensing, 59, 10022-10034, https://doi.org/10.1109/tgrs.2020.3035513, 2020.
Heid, T. and Kääb, A.: Repeat optical satellite images reveal widespread and long term decrease in land-terminating glacier speeds, The Cryosphere, 6, 467-478, https://doi.org/10.5194/tc-6-467-2012, 2012.
Herla, F., Roe, G. H., and Marzeion, B.: Ensemble statistics of a geometric glacier length model, Annals of Glaciology, 58, 130-135, https://doi.org/10.1017/aog.2017.15, 2017.
Herreid, S. and Pellicciotti, F.: The state of rock debris covering Earth's glaciers, Nature Geoscience, 13, 621-627, https://doi.org/10.1038/s41561-020-0615-0, 2020.
Howat, I. M., Porter, C., Smith, B. E., Noh, M.-J., and Morin, P.: The Reference Elevation Model of Antarctica, The Cryosphere, 13, 665-674, https://doi.org/10.5194/tc-13-665-2019, 2019.
Hugonnet, R., McNabb, R., Berthier, E., Menounos, B., Nuth, C., Girod, L., Farinotti, D., Huss, M., Dussaillant, I., Brun, F., and Kaab, A.: Accelerated global glacier mass loss in the early twenty-first century, Nature, 592, 726-731, https://doi.org/10.1038/s41586-021-03436-z, 2021.
Immerzeel, W. W., Lutz, A. F., Andrade, M., Bahl, A., Biemans, H., Bolch, T., Hyde, S., Brumby, S., Davies, B. J., Elmore, A. C., Emmer, A., Feng, M., Fernández, A., Haritashya, U., Kargel, J. S., Koppes, M., Kraaijenbrink, P. D. A., Kulkarni, A. V., Mayewski, P. A., Nepal, S., Pacheco, P., Painter, T. H., Pellicciotti, F., Rajaram, H., Rupper, S., Sinisalo, A., Shrestha, A. B., Viviroli, D., Wada, Y., Xiao, C., Yao, T., and Baillie, J. E. M.: Importance and vulnerability of the world's water towers, Nature, 577, 364-369, https://doi.org/10.1038/s41586-019-1822-y, 2019.
Ji, Q., Yang, T.-b., He, Y., Qin, Y., Dong, J., and Hu, F.-s.: A simple method to extract glacier length based on Digital Elevation Model and glacier boundaries for simple basin type glacier, Journal of Mountain Science, 14, 1776-1790, https://doi.org/10.1007/s11629-016-4243-5, 2017.
Kääb, A., Jacquemart, M., Gilbert, A., Leinss, S., Girod, L., Huggel, C., Falaschi, D., Ugalde, F., Petrakov, D., Chernomorets, S., Dokukin, M., Paul, F., Gascoin, S., Berthier, E., and Kargel, J. S.: Sudden large-volume detachments of low-angle mountain glaciers – more frequent than thought?, The Cryosphere, 15, 1751-1785, https://doi.org/10.5194/tc-15-1751-2021, 2021.
Kienholz, C., Hock, R., and Arendt, A. A.: A new semi-automatic approach for dividing glacier complexes into individual glaciers, Journal of Glaciology, 59, 925-937, https://doi.org/10.3189/2013JoG12J138, 2013.

Kienholz, C., Rich, J. L., Arendt, A. A., and Hock, R.: A new method for deriving glacier centerlines applied to glaciers in Alaska and northwest Canada, The Cryosphere, 8, 503-519, https://doi.org/10.5194/tc-8-503-2014, 2014.

Le Bris, R. and Paul, F.: An automatic method to create flow lines for determination of glacier length: A pilot study with Alaskan glaciers, Computers & Geosciences, 52, 234-245, https://doi.org/10.1016/j.cageo.2012.10.014, 2013.

Le Moine, N. and Gsell, P.-S.: A graph-based approach to glacier flowline extraction: An application to glaciers in Switzerland, Computers & Geosciences, 85, 91-101, https://doi.org/10.1016/j.cageo.2015.09.010, 2015.

Leclercq, P. W. and Oerlemans, J.: Global and hemispheric temperature reconstruction from glacier length fluctuations, Climate Dynamics, 38, 1065-1079, https://doi.org/10.1007/s00382-011-1145-7, 2011.

Leclercq, P. W., Oerlemans, J., Basagic, H. J., Bushueva, I., Cook, A. J., and Le Bris, R.: A data set of worldwide glacier length fluctuations, The Cryosphere, 8, 659-672, https://doi.org/10.5194/tc-8-659-2014, 2014.

Li, H., Ng, F., Li, Z., Qin, D., and Cheng, G.: An extended "perfect-plasticity" method for estimating ice thickness along the flow line of mountain glaciers, Journal of Geophysical Research: Earth Surface, 117, n/a-n/a, https://doi.org/10.1029/2011jf002104, 2012.

Li, X., Ding, Y., Hood, E., Raiswell, R., Han, T., He, X., Kang, S., Wu, Q., Yu, Z., Mika, S., Liu, S., and Li, Q.: Dissolved Iron Supply from Asian Glaciers: Local Controls and a Regional Perspective, Global Biogeochemical Cycles, 33, 1223-1237, https://doi.org/10.1029/2018gb006113, 2019.

Li, Y., Li, F., Shangguan, D., and Ding, Y.: A new global gridded glacier dataset based on the Randolph Glacier Inventory version 6.0, Journal of Glaciology, 67, 773-776, https://doi.org/10.1017/jog.2021.28, 2021.

Lüthi, M. P., Bauder, A., and Funk, M.: Volume change reconstruction of Swiss glaciers from length change data, Journal of Geophysical Research, 115, https://doi.org/10.1029/2010jf001695, 2010.

Machguth, H. and Huss, M.: The length of the world's glaciers – a new approach for the global calculation of center lines, The Cryosphere, 8, 1741-1755, https://doi.org/10.5194/tc-8-1741-2014, 2014.

Maussion, F., Butenko, A., Champollion, N., Dusch, M., Eis, J., Fourteau, K., Gregor, P., Jarosch, A. H., Landmann, J., Oesterle, F., Recinos, B., Rothenpieler, T., Vlug, A., Wild, C. T., and Marzeion, B.: The Open Global Glacier Model (OGGM) v1.1, Geoscientific Model Development, 12, 909-931, https://doi.org/10.5194/gmd-12-909-2019, 2019.

Melkonian, A. K., Willis, M. J., and Pritchard, M. E.: Satellite-derived volume loss rates and glacier speeds for the Juneau Icefield, Alaska, Journal of Glaciology, 60, 743-760, https://doi.org/10.3189/2014JoG13J181, 2017.

Noel, B., Jakobs, C. L., van Pelt, W. J. J., Lhermitte, S., Wouters, B., Kohler, J., Hagen, J. O., Luks, B., Reijmer, C. H., van de Berg, W. J., and van den Broeke, M. R.: Low elevation of Svalbard glaciers drives high mass loss variability, Nat Commun, 11, 4597, https://doi.org/10.1038/s41467-020-18356-1, 2020.

Oerlemans, J.: A flowline model for Nigardsbreen, Norway: projection of future glacier length based on dynamic calibration with the historic record, Annals of Glaciology, 24, 382-389, https://doi.org/10.1017/S0260305500012489 1997.

Pfeffer, W. T., Arendt, A. A., Bliss, A., Bolch, T., Cogley, J. G., Gardner, A. S., Hagen, J.-O., Hock, R., Kaser, G., Kienholz, C., Miles, E. S., Moholdt, G., Mölg, N., Paul, F., Radić, V., Rastner, P., Raup,

B. H., Rich, J., and Sharp, M. J.: The Randolph Glacier Inventory: a globally complete inventory of glaciers, Journal of Glaciology, 60, 537-552, https://doi.org/10.3189/2014JoG13J176, 2014.

Pritchard, H. D.: Asia's shrinking glaciers protect large populations from drought stress, Nature, 569, 649-654, https://doi.org/10.1038/s41586-019-1240-1, 2019.

Radić, V. and Hock, R.: Regional and global volumes of glaciers derived from statistical upscaling of glacier inventory data, Journal of Geophysical Research, 115, https://doi.org/10.1029/2009jf001373, 2010.

RGI Consortium: Randolph Glacier Inventory – A Dataset of Global Glacier Outlines: Version 6.0: Technical Report, Global Land Ice Measurements from Space, Colorado, USA, 10.7265/N5-RGI-60, 2017.

Scherler, D., Wulf, H., and Gorelick, N.: Global Assessment of Supraglacial Debris-Cover Extents, Geophysical Research Letters, 45, 11,798-711,805, https://doi.org/10.1029/2018gl080158, 2018.

Schiefer, E., Menounos, B., and Wheate, R.: An inventory and morphometric analysis of British Columbia glaciers, Canada, Journal of Glaciology, volume 54, 551-560, 2008.

Shukla, A., Garg, S., Mehta, M., Kumar, V., and Shukla, U. K.: Temporal inventory of glaciers in the Suru sub-basin, western Himalaya: impacts of regional climate variability, Earth System Science Data, 12, 1245-1265, https://doi.org/10.5194/essd-12-1245-2020, 2020.

Shukla, T. and Sen, I. S.: Preparing for floods on the Third Pole, Science, 372, 232-234, https://doi.org/10.1126/science.abh3558, 2021.

Sommer, C., Malz, P., Seehaus, T. C., Lippl, S., Zemp, M., and Braun, M. H.: Rapid glacier retreat and downwasting throughout the European Alps in the early 21(st) century, Nat Commun, 11, 3209, https://doi.org/10.1038/s41467-020-16818-0, 2020.

Stuart-Smith, R. F., Roe, G. H., Li, S., and Allen, M. R.: Increased outburst flood hazard from Lake Palcacocha due to human-induced glacier retreat, Nature Geoscience, 14, 85-90, https://doi.org/10.1038/s41561-021-00686-4, 2021.

Sugiyama, S., Bauder, A., Zahno, C., and Funk, M.: Evolution of Rhonegletscher, Switzerland, over the past 125 years and in the future : application of an improved flowline model, Annals of Glaciology, 46, 268-274, 2007.

Thogersen, K., Gilbert, A., Schuler, T. V., and Malthe-Sorenssen, A.: Rate-and-state friction explains glacier surge propagation, Nat Commun, 10, 2823, https://doi.org/10.1038/s41467-019-10506-4, 2019.

Uuemaa, E., Ahi, S., Montibeller, B., Muru, M., and Kmoch, A.: Vertical Accuracy of Freely Available Global Digital Elevation Models (ASTER, AW3D30, MERIT, TanDEM-X, SRTM, and NASADEM), Remote Sensing, 12, https://doi.org/10.3390/rs12213482, 2020.

Vargo, L. J., Anderson, B. M., Dadić, R., Horgan, H. J., Mackintosh, A. N., King, A. D., and Lorrey, A. M.: Anthropogenic warming forces extreme annual glacier mass loss, Nature Climate Change, 10, 856-861, https://doi.org/10.1038/s41558-020-0849-2, 2020.

Winsvold, S. H., Andreassen, L. M., and Kienholz, C.: Glacier area and length changes in Norway from repeat inventories, The Cryosphere, 8, 1885-1903, https://doi.org/10.5194/tc-8-1885-2014, 2014.

Wu, K., Liu, S., Jiang, Z., Liu, Q., Zhu, Y., Yi, Y., Xie, F., Ahmad Tahir, A., and Saifullah, M.: Quantification of glacier mass budgets in the Karakoram region of Upper Indus Basin during the early twenty-first century, Journal of Hydrology, 603, https://doi.org/10.1016/j.jhydrol.2021.127095, 2021.

Xia, W.: An Automatic Extraction Method of Glacier Length Based on Voronoi Algorithm - A Pilot Study in the Sanjiangyuan Region, College of Urban and Environmental Science, Northwest University, Xi'an, Shannxi, 2020.

Yang, B. Y., Zhang, L. X., Gao, Y., Xiang, Y., Mou, N. X., and Suo, L. D. B.: An integrated method of glacier length extraction based on Gaofen satellite data, Journal of Glaciology and Geocryology, 38, 1615-1623, https://doi.org/10.7522/j.issn.1000-0240.2016.0189, 2016.

Yao, X. J., Liu, S. Y., Zhu, Y., Gong, P., An, L. N., and Li, X. F.: Design and implementation of an automatic method for deriving glacier centerlines based on GIS, Journal of Glaciology and Geocryology, 37, 1563-1570, https://doi.org/10.7522/j.issn.1000-0240.2015.0173, 2015.

Zemp, M., Huss, M., Thibert, E., Eckert, N., McNabb, R., Huber, J., Barandun, M., Machguth, H., Nussbaumer, S. U., Gartner-Roer, I., Thomson, L., Paul, F., Maussion, F., Kutuzov, S., and Cogley, J. G.: Global glacier mass changes and their contributions to sea-level rise from 1961 to 2016, Nature, 568, 382-386, https://doi.org/10.1038/s41586-019-1071-0, 2019.

Zhang, D. and Zhang, S.: A new global dataset of mountain glacier centerline and length, Science Data Bank, https://doi.org/10.11922/sciencedb.01643, 2022.

Zhang, D., Yao, X., Duan, H., Liu, S., Guo, W., Sun, M., and Li, D.: A new automatic approach for extracting glacier centerlines based on Euclidean allocation, The Cryosphere, 15, 1955-1973, https://doi.org/10.5194/tc-15-1955-2021, 2021.

Zheng, G., Allen, S. K., Bao, A., Ballesteros-Cánovas, J. A., Huss, M., Zhang, G., Li, J., Yuan, Y., Jiang, L., Yu, T., Chen, W., and Stoffel, M.: Increasing risk of glacial lake outburst floods from future Third Pole deglaciation, Nature Climate Change, 11, 411-417, https://doi.org/10.1038/s41558-021-01028-3, 2021.

Zhou, S., Yao, X., Zhang, D., Zhang, Y., Liu, S., and Min, Y.: Remote Sensing Monitoring of Advancing and Surging Glaciers in the Tien Shan, 1990–2019, Remote Sensing, 13, https://doi.org/10.3390/rs13101973, 2021a.

Zhou, Y., Li, X., Zheng, D., Li, Z., An, B., Wang, Y., Jiang, D., Su, J., and Cao, B.: The joint driving effects of climate and weather changes caused the Chamoli glacier-rock avalanche in the high altitudes of the India Himalaya, Science China Earth Sciences, 64, 1909-1921, https://doi.org/10.1007/s11430-021-9844-0, 2021b.